Bioengineered niches that recreate physiological extracellular matrix organisation to support long-term haematopoietic stem cells

Hannah Donnelly[1], Ewan Ross[1], Yinbo Xiao[1], Rio Hermantara[2], Aqeel Taqi[2], Annie Cheng[3], Nikhil Jain[4], Christopher West[5], Bruno Peault[5], Adam G. West[2], Manuel Salmeron-Sanchez[3*], Matthew J. Dalby[1*].

[1]Centre for the Cellular Microenvironment, School of Molecular Biosciences, College of Medical, Veterinary and Life Sciences, Joseph Black Building, University of Glasgow, Glasgow, G12 8QQ, United Kingdom.
[2]School of Cancer Sciences, Wolfson Wohl Cancer Research Centre, University of Glasgow, Glasgow, G61 1QH, United Kingdom.
[3]Centre for the Cellular Microenvironment, Division of Biomedical Engineering, School of Engineering, University of Glasgow, Glasgow, G12 8QQ, United Kingdom.
[4]Institute of Inflammation and Ageing, University of Birmingham, Queen Elizabeth Hospital, Birmingham, B15 2WB, United Kingdom.
[5]MRC Centre for Regenerative Medicine, The University of Edinburgh, Edinburgh, EH16 4UU, United Kingdom.

* Corresponding authors:
matthew.dalby@glasgow.ac.uk
manuel.salmeron-sanchez@glasgow.ac.uk

Abstract

Long-term reconstituting haematopoietic stem cells (LT-HSCs) are used to treat blood disorders via allogeneic stem cell transplantation (alloSCT), to engraft and repopulate the blood system. The very low abundance of LT-HSCs and their rapid differentiation during in vitro culture hinders their clinical utility. Previous developments using stromal feeder layers, defined media cocktails, and bioengineering have enabled HSC expansion in culture, but of mostly short-term HSCs (ST-HSC) and progenitor populations at the expense of naïve LT-HSCs. Here, we report the creation of a bioengineered LT-HSC maintenance niche that recreates physiological extracellular matrix organisation, using soft collagen type-I hydrogels to drive nestin expression in perivascular stromal cells (PerSCs or pericytes). We demonstrate that nestin, which is expressed by HSC-supportive bone marrow stromal cells, is cytoprotective and, via regulation of metabolism, is important for HIF-1α expression in PerSCs. When CD34^{+ve} HSCs were added to the bioengineered niches comprising nestin/HIF-1α expressing PerSCs, LT-HSC numbers were maintained with normal clonal ability and without media supplementation. We provide proof-of-concept that our bioengineered niches can support the survival of CRISPR edited HSCs. Successful editing of LT-HSCs ex vivo can have potential impact on the treatment of blood disorders.

Haematopoietic diseases are a major healthcare burden, costing the UK economy £4B pa[1], with leukaemia therapy typically requiring multiple courses of intensive chemotherapy, often followed by allogeneic haematopoietic stem cell (HSC) transplant (alloSCT). AlloSCT transplantation replaces a patients hematopoietic cells through myeloablation of host bone marrow, followed by reconstitution with transplanted donor cells to restore normal immune function[2]. Given that alloSCT has been demonstrated to be an increasingly efficacious therapy for not only leukaemias but also for primary immuno-deficiencies and autoimmune conditions, there is an increasing demand for HSC transplantation and for matched donors[3], particularly in the context of an aging and ethnically diverse population. However, we currently cannot meet the clinical demand as there is no defined and regulated expansion methodologies for bone marrow (BM) HSCs meaning that we are reliant on donation. Furthermore, engraftment of HSCs can be limited following alloSCT, leading to prolonged haemopoietic recovery time post-transplantation which is a major cause of transplant failure and patient mortality[2].

Long-term (LT)-HSCs are critically important for therapy as they engraft long-term to repopulate the blood system following alloSCT[4]. However, LT-HSCs represent just 0.01 - 0.04% of the mononuclear bone marrow population[5] and they rapidly differentiate towards short-term (ST)-HSCs and progenitor cells upon their culture in vitro, which provide only temporary engraftment and myeloid/lymphoid progenitors[4,5]. Therefore, maintaining and, ultimately, expanding LT-HSCs ex vivo has become a major focus of research. Several culture systems, such as Dexter cultures[6], and the use of cytokines[7] and small molecules[8], have successfully expanded heterogenous CD34+ HSCs in vitro but with the concomitant loss of naïve LT-HSCs, producing populations with clonal heterogeneity[9]. Subsequent transplantation studies and phase I/II clinical trials (with e.g. the small molecule SR1) have shown that most engrafted cells are ST-HSCs and their subsequent progenitors[10].

The inability to maintain LT-HSCs, or to support their self-renewal, in these systems is likely to be related to the lack of the many physical and functional signalling components of the highly complex bone BM microenvironment, where the expansion and differentiation of HSCs and other hematopoietic cells are regulated[11]. To maintain LT-HSCs ex vivo, there needs to be defined conditions which allow activation and proliferation without inducing differentiation to ST-HSC and subsequent committed progenitors[4]. This has proven to be difficult to achieve in a heterogenous BM cell population, especially when a single parameter, such as one signalling pathway, is targeted with small molecules[8]. Multiple cell types also interact in the BM and co-operate with each other through cell-cell adhesion and paracrine signals, such as mesenchymal stromal cells (MSCs) and perivascular stromal cells (PerSCs)[12–16]. Other critical cellular factors in the BM stem cell niche are C-X-C motif chemokine 12 (CXCL12, also known as stromal cell-derived factor 1 (SDF1)) abundant reticular (CAR) cells[17], and bone-forming osteoblasts[15,16]. All are implicated in LT-HSC maintenance, while nestin^{+ve} perivascular stromal cells are specifically implicated in LT-HSC self-renewal in murine studies[12,13,18]. This observation of nestin^{+ve} stromal cells being important to LT-HSC phenotype is interesting as soft materials, such as hydrogels, have been implicated in the expression of nestin in MSCs[19]. While originally this was ascribed to a neural phenotype[19], we hypothesise this seminal observation can be important in engineering of a niche-stromal phenotype and that stromal nestin expression will provide key niche functionalities.

Indeed, the BM itself is a soft material, comprising extracellular matrix (ECM)[20] with a Young's modulus of 1 – 10^4 Pa[21], that interfaces with hard materials, such as the bone lining (endosteal) surfaces[22] and the arterioles and sinusoidal capillaries, to which PerSCs adhere, affecting their mechanotransductive signalling and phenotype[13,23]. Growth factors (GFs) and cytokines interact with ECM's structural proteins, such as fibronectin (FN), facilitating synergistic signalling between ECM-adhering integrin receptors and GF receptors, further influencing the stromal phenotype[24]. The BM niche also features hypoxic environments[25]. The endosteal niche was traditionally considered to be highly hypoxic, but it has been shown that the endosteal surface is perfused with a network of oxygenated arterioles[13,25]. By contrast, the central cavity is filled with more hypoxic sinusoids[13,25]. Hypoxic conditions can influence cell phenotypes, with hypoxic culture conditions reducing stromal cell proliferation and maintaining their stem cell phenotype[26]. Indeed, hypoxia inducible factor (HIF) expression by stromal cells is believed to be important for their HSC regulatory capacity[27].

We propose that multiple elements of the BM's complexity needs be recapitulated in vitro to maintain LT-HSCs. Numerous in vitro models of the BM niche are currently in development. Some integrate multiple types of support cells[18,28], 3D hydrogels[29,30] and scaffolds[31], while others employ perfusion cultures[32], and combine different approaches on organ-on-chip devices[33]. While these emerging models inform our understanding of the human BM during injury or neoplasia[33], and of $CD34^{+ve}$ HSC expansion[18,28], they have their limitations. Many use murine $CD34^{+ve}$ cells, despite the notable differences between human and murine HSC regulation[34], others measure expansion based on $CD34^{+ve}$ numbers rather than on the LT-HSC population, while some models are complex or hard to use or recover cells from[4]. To our knowledge, there is no reported system that focuses on enhancing human LT-HSC maintenance in a simple-to-use, practical, system. Such a system could inform on both maintenance of LT-HSCs for therapeutic use as well as providing a platform to test novel drugs or gene editing of HSCs in vitro, that can offer novel therapeutic cell based therapies to treat malignant and non-malignant blood disorders.

In this study, we employ bioengineering approaches in order to direct the physiology of the stromal feeder layer and enhance its ability to support and maintain LT-HSC in culture. We provide a polymeric surface that controls FN fibril formation allowing both an adhesive and direct GF signal to stromal cells[35,36], as well as a soft material to induce nestin expression to stimulate the stromal HSC-supportive phenotype[12,13,18]. Our findings show that nestin expression, linked to changes in respiration, are central to enhanced LT-HSC maintenance. We further demonstrate that our bioengineered niches have the potential to support improved survival of CRISPR edited HSCs in this clinically important population.

Results

Recapitulating the endosteal surface in vitro

The BM niche has different putative regions with different roles in HSC regulation. The sinusoidal (central marrow cavity) niche is associated with sinusoidal capillaries and is more hypoxic relative to other BM regions[25], and self-renewing HSCs are considered to reside there[14]. The endosteal surface, which is in close proximity to a large network of oxygenated arterioles, is believed to retain a more quiescent pool of HSCs[12,13,25,37,38]. The BM also has a dense ECM network, the constituents of which are exchanged between the endosteal and

sinusoidal niches. At the endosteal surface, the ECM is stiffer and fibronectin (FN) rich. Towards the sinusoidal niches in the central BM cavity, the ECM becomes progressively less stiff and more collagen- and laminin-rich [39,40]. The conformation of ECM proteins, as well as their type and density, all strongly influence BM cell interactions[41].

Our previous work has shown that fibrillar FN can efficiently bind and present BMP-2 (bone morphogenetic protein 2, an osteogenic GF) to promote osteogenesis in MSCs in vitro[35] and fracture healing in vivo[36]. We have adapted these findings here to recreate the ECM properties of the more-quiescent endosteal niche. Poly(ethyl acrylate) (PEA) leads to the spontaneous unfolding of FN (Figure 1a), as visualised with AFM (Figure 1b). This cell-driven unfolding process leads to the exposure of key binding domains in the FN molecule[42]. Chemically similar poly(methyl acrylate) (PMA) is used as a reference polymer here, on which FN is adsorbed and maintained in a globular conformation (Figure 1b). PMA behaves similarly to PEA in terms of surface wettability and stiffness[43], but with increased adsorption of FN (Figure 1c). The fluorescent detection of antibodies that recognise total FN (Figure 1d), FN's arginine-glycine-aspartic acid (RGD)-containing HFN7.1 integrin-binding domain (Figure 1e), and its P5F3 GF-binding domain (Figure 1f) demonstrates the significantly increased availability of these FN domains when absorbed on PEA, relative to PMA. The P5F3 domain of FN in particular has high binding affinity for several GF families[44]. Here, we show that BMP-2 binds to PEA-FN (Figure 1g). Although similar amounts of BMP-2 also bind to PMA, our previous work has shown that BMP-2 does not co-localise with FN on PMA, leading to its faster release[35,36]. Thus, in this study, we use PEA to present FN and BMP-2 to recreate the milieu of the endosteal surface that supports HSC quiescence (maintenance) in our BM model.

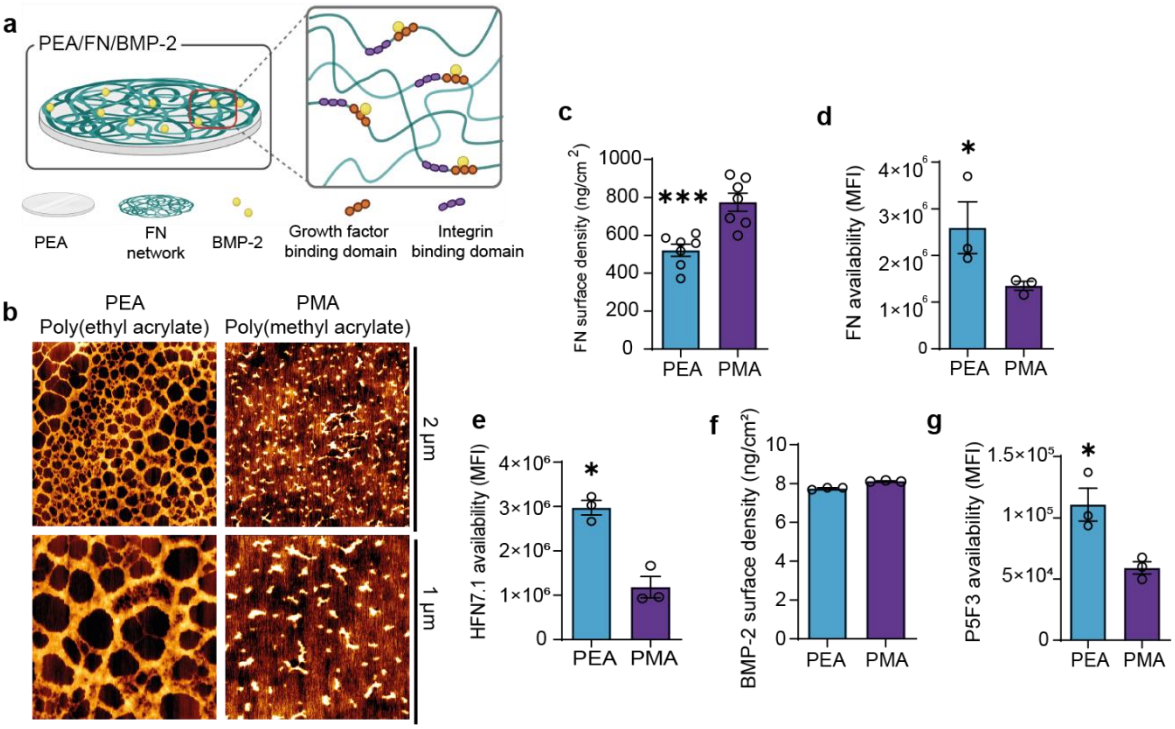

***Figure 1 | Control of the protein interface using acrylate polymers. a**, Schematic of the PEA system. **b,** AFM images showing fibronectin (FN) spontaneously forms networks on PEA surfaces but not on PMA. **c,** Surface density of FN on surfaces coated with 20 µg/mL solution of PEA and PMA, showing that more FN adsorbs to PMA (n = 7). The availability of **d,** total FN; **e,** FN HFN7.1 domain (RGD-binding); and **f,** P5F3 domain (growth factor*

(GF)-binding), was assessed using in-cell western analysis. Data shows the increased availability of RGD- and GF-binding FN domains on PEA. ***g,*** *Surface density of BMP-2 on PEA-FN and PMA-FN, as assessed by ELISA. 50 ng/mL of BMP-2 was loaded onto the surface, leading to ~8 ng/cm^2 of BMP-2 sequestered on both PEA and PMA (**d - g,** n = 3).* ***c – g,*** *Graphs show mean ± SEM, *= p<0.05, ***= p<0.001 determined by Mann-Whitney t-test, n = 3 material replicates.*

Control of PerSC phenotype

The stromal population of the BM niche is highly heterogeneous[11]. Reported expression of markers, such as nestin, neural-glial antigen 2 (NG-2) and leptin receptor (LepR), indicate that perivascular and mesenchymal stromal cells have a phenotype that supports HSC regulation[12–14]. Here, we focus on the LT-HSC regulating perivascular stromal cells that line the endosteal arterioles[12,13,18], and on nestin. Nestin is a cytoskeletal intermediate filament (IF) protein traditionally associated with neural progenitor cells[45]. In vivo murine BM studies have shown that nestin^{+ve} PerSCs express high levels of factors involved in HSC maintenance, such as CXCL12 and stem cell factor (SCF)[38]. Previous seminal work has also shown that stromal cells express nestin in response to soft materials[19]. We therefore used low-stiffness collagen hydrogels, a major constituent of the BM ECM[39], to study the role of nestin expression in human PerSCs and to investigate how this influences their interactions with HSCs in vitro.

The collagen gels, with a Young's modulus of ~80 Pa to mimic BM HSC niche stiffness[21], were overlayed onto PerSCs cultured on PEA/FN/BMP-2 surfaces (Figure 2a, b). We also used PEA/FN/BMP-2 with a lowered oxygen tension (1% O_2, hypoxia), since hypoxia is considered to be important for maintaining the stromal HSC supporting phenotype in the BM environment[25] (Figure 2a). We observed in our bioengineered PEA/FN/BMP-2 niches with hydrogels (denoted as +gel) that nestin was significantly upregulated by day 7 in PerSCs (Figure 2c), with enhanced nestin expression continuing to day 14 (supplementary Figure 1a). By contrast, nestin was expressed at a basal level in PEA/FN/BMP-2 niches without hydrogels (denoted as -gel), in the PEA/FN/BMP-2 hypoxic niches and in PMA/FN/BMP-2 niches with and without gels (supplemetary Figure 1a). We used PerSCs on glass coverslips as a culture control since they do not attach to highly hydrophobic PEA without a protein interface (Fig 2c,d,e and f). Thus, nestin expression was induced only when the gel was included on PEA-unfolded FN. Nestin is a type IV IF protein incapable of self-polymerisation. It, therefore, co-polymerises with other type II and IV IFs [45]. We therefore examined vimentin expression, as an IF protein expressed in mesenchymal-lineage cells, and found no significant differences in vimentin expression or its morphology (Figure 2d).

Next, PerSCs were treated with brefeldin A for the final 24h of culture to prevent protein export and SCF levels were monitored by immunofluorescence. SCF production correlated with the observed increase in nestin expression in PEA +gel niches (Figure 2e, supplementary figure 1b). CXCL12 expression was also detected in PerSCs on all substrates, with no significant differences between the bioengineered models (supplementary Figure 1c).

Phenotypic analysis by flow cytometry of the different environments showed that PerSCs in +gel niches expressed important stromal niche markers CD90, NG2, CD146 and CD51, but that expression was lost in -gel niches[13,16,18] (Figure 2f). Interestingly, the introduction of hypoxia also led to expression of these markers, and also increased expression of LepR. LepR is a marker of stromal cells that line hypoxic sinusoids, and supports our attempt to recreate an

arteriolar/endosteal niche in which stromal cells are reported to be nestin^{+ve}/LepR^{-ve} [12,14,38] (Figure 2f).

Next, we performed RNA-seq on PerSCs cultured in the PEA/FN/BMP-2 -gel, +gel and hypoxic niches. RNA-seq identified transcripts related to niche (Figure 2g) or regulation of differentiation (Figure 2h). Importantly, cells from the +gel niche had an up-regulation of niche genes and a concomitant down-regulation of differentiation genes, compared to control and other conditions (-gel and hypoxia) (Figure 2g, h). The known functions of these genes are listed in supplementary Tables 1 & 2.

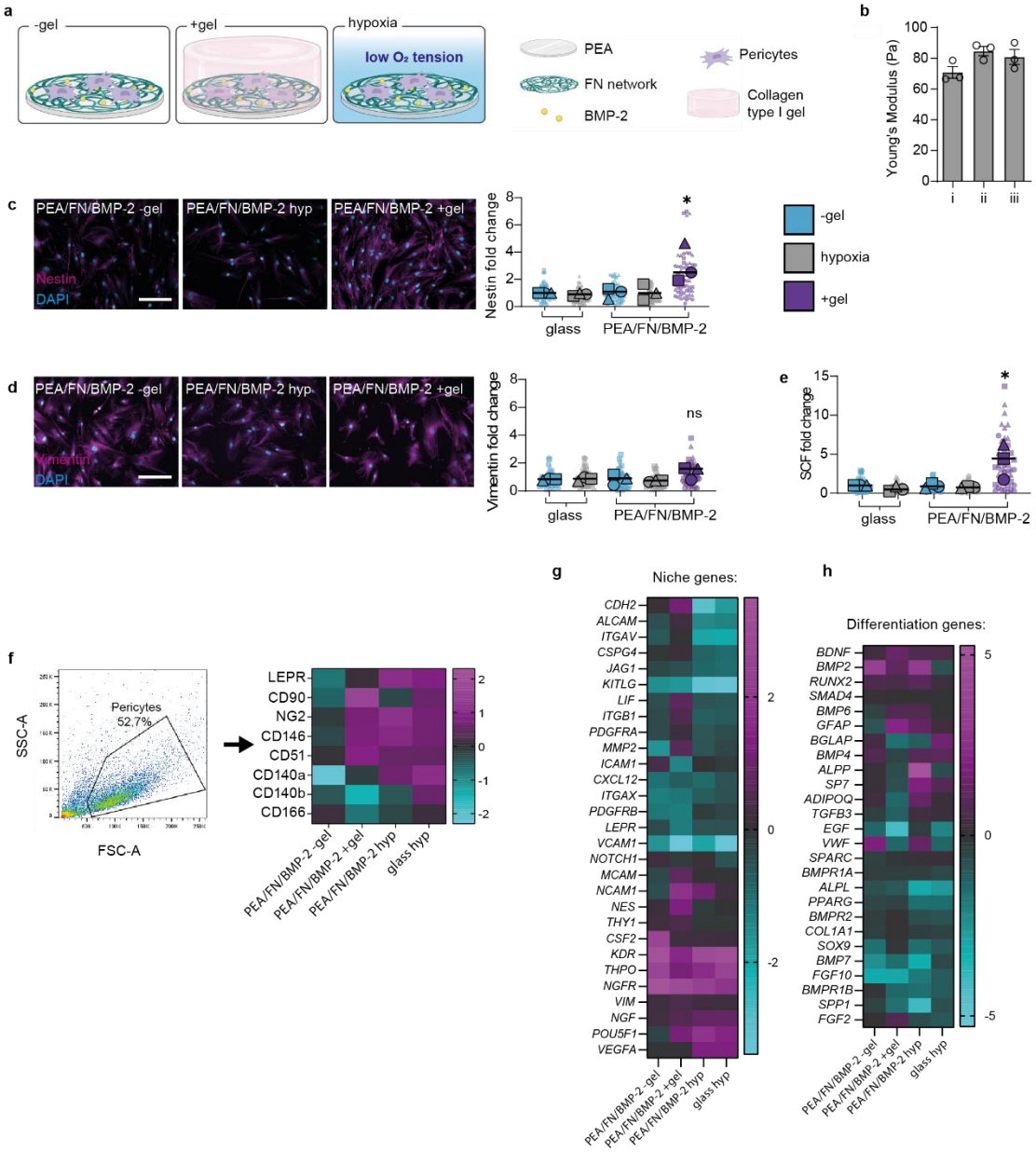

Figure 2 | Investigating bioengineered niches that support BM stromal phenotypes. a, *Schematic of niche model set-up.* ***b,*** *Young's modulus of collagen type I gels used in +gel niches. I-iii represent 3 independent batches of gels formulated. The average Young's modulus was 78.8 Pa; no statistical significance was observed, as determined by one-way ANOVA followed by Tukey's multiple comparison.* ***c,*** *Representative images of changes in nestin expression evaluated by immunofluorescence at day 7. Scale bar is 100 µm, magenta = nestin, cyan = DAPI.* ***D,*** *Representative images of vimentin expression, as evaluated by immunofluorescence microscopy at day 7, shows no significant difference between models., scale bar is 100 µm, magenta = vimentin, cyan = DAPI.* ***e,***

*SCF production in bioengineered models, in which PerSCs were cultured for 14 days, with brefeldin A added for the final 24h to inhibit intracellular protein transport. Graphs in **c-e** show mean integrated intensity of marker as fold change to glass control; -gel = blue, +gel = purple, hypoxia = grey. Each point represents an individual field. N = 3-4 material replicates, for 3 independent experiments with different donor cells (each donor represented by a different shape), *= p<0.05, ns= non-significant, determined by one-way ANOVA followed by Tukey's multiple comparison test. **f,** Assessment of PerSC phenotype after 14 days culture in niche models. Heatmap shows fold change over control (glass) of median fluorescent values obtained by flow cytometry from 6 pooled material replicates from 3 independent experiments with different donor cells. At least 5000 cells were collected per sample. **g** and **h,** RNA-seq was performed on PerSCs from niche models after 7 days and fold changes in gene expression relative to glass control are shown as a heatmap. N = 6 pooled material replicates from 1 donor.*

Using principal component analysis (PCA), the -gel/+gel/hypoxic conditions were clearly distinguishable from each other by RNA-seq (Supplementary Figure 2a). Analysis of significant gene changes revealed that most unique changes occurred in the +gel niche, and that the +gel and hypoxic models had more changes in common, relative to the -gel model (Figure 3a). Gene ontology (GO) clustering analysis indicates that a range of changes occurred in response to the different engineered ECM environments (-gel / +gel). Changes in integrins, adhesion molecules, ECM interactions, cytoskeleton and to the BMP-2 milieu, were evident in response to these ECM changes, as were changes to members of the canonical BMP signalling family, including TGFβs and SMADs (Figure 3b). Clustering analysis of the four top networks of actin cytoskeleton, cell adhesion and ECM, illustrated that in the +gel niches, the PerSCs had decreased levels of cytoskeletal transcripts and increased levels of cell adhesion and ECM transcripts, compared to the -gel models (Figure 3c). The hypoxic niche, however, both up-regulated and down-regulated ECM transcripts, and strongly repressed adhesion and actin related transcripts, relative to the other models (Figure 3c).

Another feature of the naïve stromal stem cell phenotype is the ability to modulate the immune system[46]. We therefore compared the expression profiles of inflammation-related marker genes across the three different niches. Several markers up-regulated in PerSCs in the +gel niche, compared to the -gel model, are implicated in immunomodulatory properties of the stromal phenotype, including interleukin 6 (IL-6)[47], prostaglandin-endoperoxide synthase 2 (PTGS2), prostaglandin E2 receptor 2 (PTGER2)[48], CD44, tumour necrosis factor α-induced protein 3 (TNFAIP3) [49] and ephrin type-A receptor 2 (EPHA2)[50] (Figure 3d). PerSCs in the hypoxic and -gel models showed reduced expression of these immunomodulatory transcripts, with little difference between them, whereas +gel niches led to enhanced expression of these transcripts when compared to both -gel and hypoxic niches (Figure 3d). Together, these findings help demonstrate that a naïve perivascular stromal cell phenotype is retained in the +gel niches.

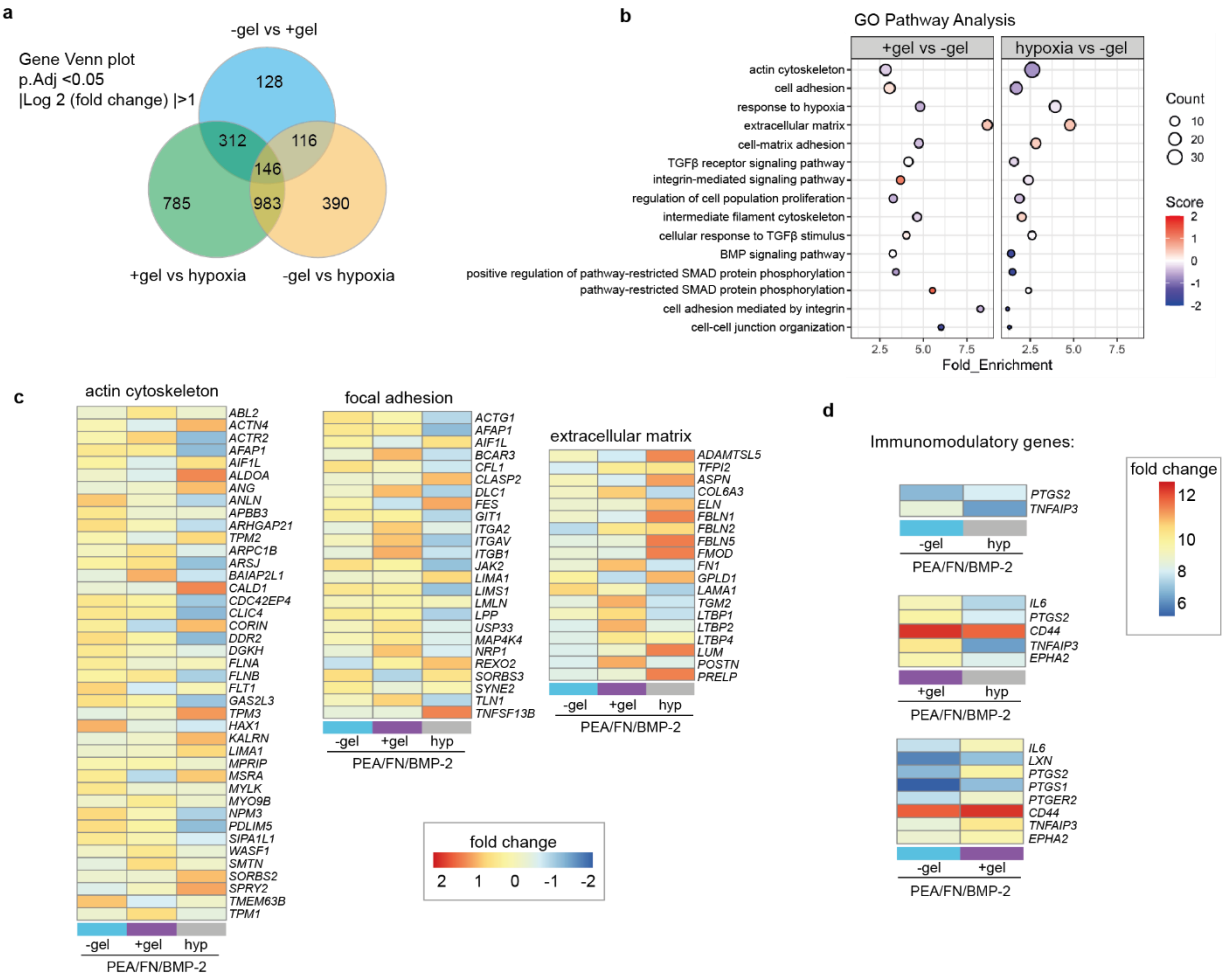

Figure 3 | Investigating bioengineered niches that support PerSC phenotype. *RNA-seq was performed on PerSCs isolated from the bioengineered models at day 7.* ***a****, Venn plot shows differentially expressed genes (based on passing a threshold of adjusted p-value <0.05 and log2 fold change > 1).* ***b****, GO enrichment analysis for differentially expressed transcripts based on false discovery rate (FDR) ≤0.05 linked to pathways involved in ECM, cell adhesion and cytoskeleton. Results indicate that the cells differentially re-organise ECM relevant gene expression in response to the +gel niche or hypoxic environments. Differentially expressed genes in each of these pathways were extracted and z-scored changes are shown in the heatmaps.* ***c****, Expression profiles of genes involved in ECM, cell adhesion and cytoskeleton. In the hypoxic model, ECM-related transcripts are increased while adhesion- and cytoskeleton-related transcripts are decreased. In the +gel niche, ECM and adhesion related transcripts are more subtly increased while cytoskeleton transcripts are decreased.* ***d****, Immunomodulatory transcript expression, showing similar expression profiles in the hypoxic and -gel models, and up-regulated transcripts in the +gel niches. For RNA-seq, n=3 6 pooled material replicates from 1 donor.*

Metabolic regulation in the BM niche

In order to elucidate further the role of hypoxia in the BM niche, we investigated the role of hypoxia and stiffness on stromal niche phenotypes by using our modular platform to compare the effects of hypoxia in our bioengineered models. HIF1α is a master regulator of metabolism. It regulates both glycolysis and oxidative phosphorylation, including anaerobic glycolysis[51]. As such, we evaluated the expression pattern of HIF1α in PerSCs in our bioengineered niches after 3 days of culture. HIF1α is constitutively produced but is hydroxylated in normoxia that inhibits its transcriptional activity and targets it for ubiquitination and degradation in most cells[51]. However, in hypoxia, it becomes stable, translocates to the nucleus and activates the transcription of hypoxia-responsive genes. We,

therefore, chose to investigate nuclear expression of HIF1α (Figure 4a). By this measure, all three bioengineered models led to increased nuclear expression of HIF1α protein in PerSCs. Interestingly, however, cells in the +gel niches displayed significantly more nuclear HIF1α, expression compared to the -gel and hypoxic models; the +gel niche also supported PerSCs with the most niche-like phenotype (Figure 2c-h).

Although some hypoxic response genes are up-regulated in PerSCs in the +gel niches (supplementary Figure 2c), our investigation of HIF1α downstream targets, such as of VEGF (Figure 4b), lactate and lactate dehydrogenase (LDH) (supplementary Figure 3), did not reveal an increase in expression. To determine if the PerSCs in the +gel niches were experiencing low oxygen tension, we next used pimonidazole, a hypoxia probe. The probe revealed that while PerSCs cultured in the low oxygen tension models are clearly hypoxic, cells in the -gel models and +gel niches were not (Figure 4c). This indicates that PerSCs in the +gel niche that were expressing nuclear HIF1α were not doing so in response to lowered oxygen tension.

To identify changes in the metabolism of PerSCs in the niche models, liquid chromatography-mass spectrometry (LC-MS) was performed to identify alterations in the metabolome at 7 and 14 days of culture. PCA of all metabolites demonstrated that all three culture conditions clustered with no overlap (Figure 4d). Then, focussing only on glycolysis and TCA cycle metabolites (Figure 4e), revealed an expected increase in clusters of glycolytic metabolites in the hypoxic model, as well as the upregulation of TCA-associated metabolites in the -gel model, as would be expected with active differentiation[52]. Interestingly, for the +gel niche, we observed a general down-regulation of glycolysis and oxidative phosphorylation rather than an increase in glycolysis (Figure 4e).

HIF activity in non-hypoxic conditions is a distinguishing feature of the Warburg effect, in which cancer cells switch to rely on oxidative glycolysis to generate energy[53]. The metabolic profile of PerSCs cultured in the +gel niche appears to be more quiescent than glycolytic, however. This finding was confirmed by tracing the conversion of C^{13} labelled glucose using LC-MS in PerSCs (Figure 4f). In the +gel niches, PerSCs still retained significantly more labelled glucose compared to other conditions, indicative of lowered respiration. In the -gel models, significantly less glucose was detected at the end of the analysis, and it was not reduced to pyruvate or lactate but there was an increase in ATP levels, indicative of more normal respiration (Figure 4e). In hypoxic models, significant levels of C^{13} labelled pyruvate and lactate remained in the PerSCs, indicative of anaerobic respiration, as would be expected[53]. Taken together, these observations indicate that PerSCs in the +gel niche are not responding as if in hypoxic conditions, but are attenuating respiration. This is despite the increased expression and prolonged nuclear presence of HIF1α, which may be acting in a BM niche-specific role.

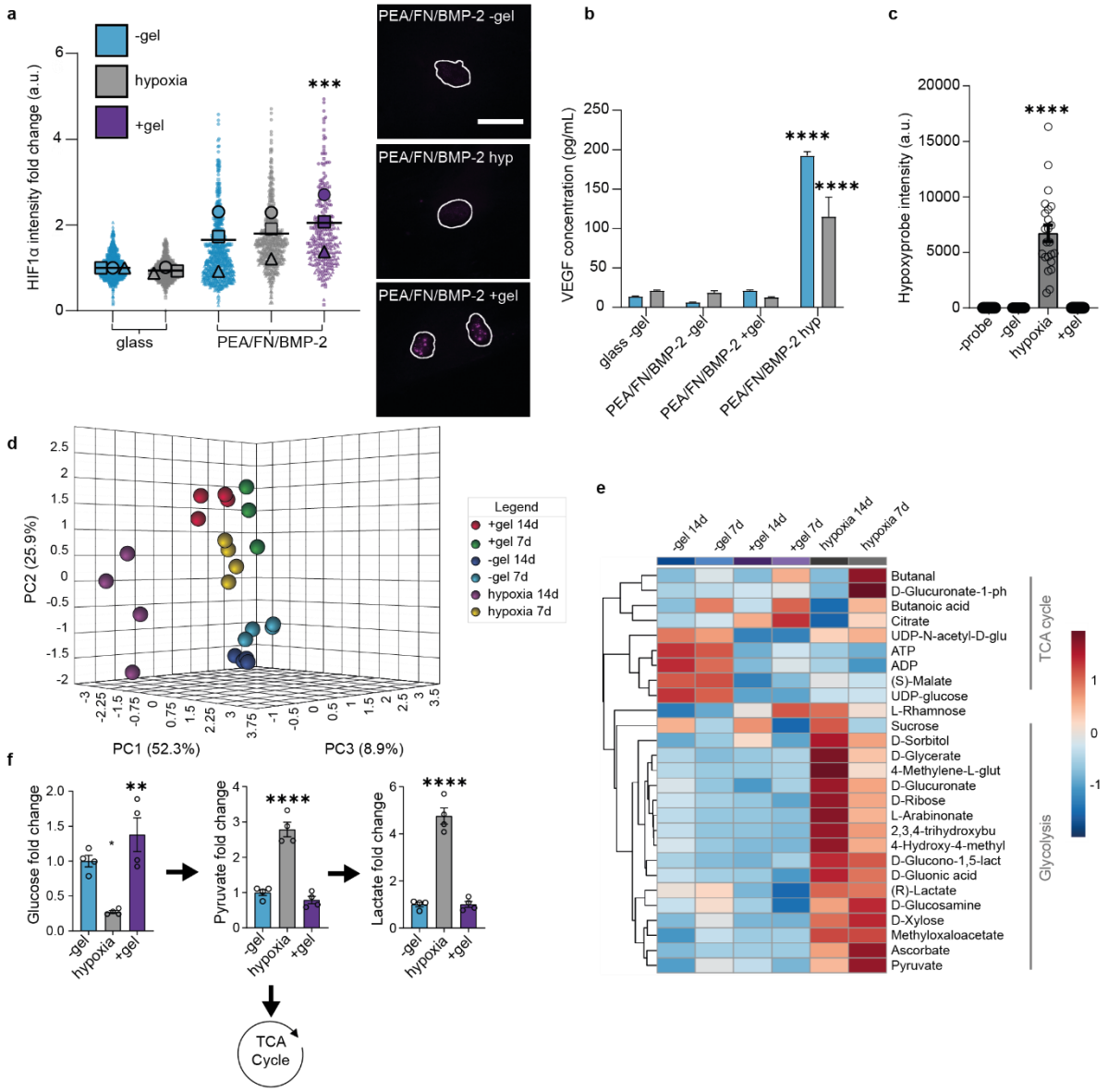

Figure 4 | Bioengineered niches promote a hypoxic-like metabolic phenotype. a*, Nuclear HIF1α levels were compared at day 3 by immunofluorescence microscopy. HIF1α levels increased in cells in all models, and significantly increased in +gel niches. Representative images are shown, magenta = HIF1α, white shows nuclei outline based on DAPI staining, scale bar = 20 µm. Graph shows means from 3 material replicates for 3 independent experiments with different donor cells. Each individual point represents 1 nuclei measurement with shape corresponding to mean.* ***b****, HIF1α downstream analysis, in which VEGF was measured from cell supernatant by ELISA on day 7 and 14, graph shows mean +SEM for 3 material replicates.* ***c****, Hypoxia was indicated when PerSCs were cultured in hypoxic but not in the +gel niches. Integrated intensity of hypoxyprobe for immunofluorescence images shown on graph, bar is mean ±SEM, each point represents 1x image field/number nuclei, n=4 material replicates.* ***d,*** *LC-MS metabolome analysis. Principal component analysis (PCA) of PEA/FN/BMP-2 models. PerSCs were cultured for 7 and 14 days. All detectable metabolites were subject to PCA. Each point represents 1 replicate (n= 3 or 4 material replicates). The PCA plot shows distinct clustering based on model and time point. PC1 separates both time points, whereas PC2 separates model condition. Hypoxic and +gel niches showed similar clustering in PC1.* ***e,*** *Glycolytic and TCA cycle metabolite profile in the bioengineered models. Heatmap shows group averages of* $\log_{10}$ *transformed peak intensities Ward clustered of each replicate at 7 and 14 days from LC-MS. Glycolysis related metabolites show increased abundance in PEA/FN/BMP-2 hypoxic conditions at 7 and 14 days, whereas TCA cycle metabolites are increased in -gel conditions at 7 and 14 days. The +gel niches show a similar down regulation of TCA cycle-associated metabolites as for hypoxic samples, but glycolysis associated metabolites are also down-regulated. N =3 for +gel 7 d, n=4 for all other samples.* ***f,*** *PerSCs were seeded for 7 days in the bioengineered models in the presence of* $^{13}C_6$*-glucose for 72h and LC-MS*

*was then used to measure the conversion and abundance of $^{13}C_6$-labelled metabolites in the glycolysis pathway. Graphs show a fold change relative to $^{13}C_6$-labelled metabolites in PerSCs cultured in the -gel model. Graphs show means ± SEM, n=4 material replicates. All statistics by one-way ANOVA with Tukey multiple comparisons test *p< 0.05, **p<0.001, **** p< 0.0001.*

Nestin is required for metabolic regulation in niches

Little is known about why nestin is highly expressed in BM niche stromal cells. We have already shown that while nestin levels are increased in +gel niches (Figure 2c), IFs (as measured using vimentin) are not (Figure 2d). To confirm this observation, we assessed the incorporation of nestin into IF networks using an antibody against p(Thr316)-nestin. This site, when phosphorylated, drives disassembly of nestin from IF fibres[54]. We observed a significant up regulation of p(Thr316) nestin in PerSCs in the +gel niche, indicating that not all nestin is incorporated into the cytoskeleton. This suggests that the function of nestin in stromal cells in our engineered BM niche does not entirely depend on its structural involvement in the cytoskeleton (Figure 5a).

Because of our HIF1α observation and because soluble nestin has been linked to cytoprotection in other cell types[54–56], we next investigated two possibilities: (1) that nestin expression is linked to the HIF1α positive PerSC phenotype, and (2) that nestin is linked to cytoprotection. Linking PerSC nestin expression and cytoprotection is perhaps important as naïve stromal cells are linked to increased caspase expression (involved in regulation of apoptosis), and enhanced killability[57] and so perhaps these cells need to be protected by their niche. We further note that enhanced killability has been linked to better immunosuppressive outcomes when using stromal cells in transplant procedures[57].

To address these questions, nestin expression was reduced by siRNA knock-down in PerSCs to test links between HIF1α expression and cytoprotective effects (Figure 5b). Interestingly, in the +gel niche, nestin knock-down led to a concomitant decrease in the levels of nuclear-localised HIF1α, demonstrating a link between nestin and HIF1α (Figure 5c). We note that a recent study indicated that nestin binds to HIF1α to protect it from degradation and showed nestin knockdown leads to loss of HIF1α, as we show here[58]. To evaluate if this link was involved in cytoprotection, oxidative stress and apoptosis was induced in PerSCs by exposure to hydrogen peroxide and changes in viability measured using propidium iodide (PI) uptake. In the +gel niches, where PerSCs express high levels of nestin, cell death in response to oxidative stress was low (Figure 5d). Reducing nestin by siRNA knock-down resulted in an increased sensitivity to oxidative stress, with a significant increase in PI positive cells observed, even for cells in +gel niches (Figure 5e; note that all conditions are with H_2O_2). These results align with reports on the effects of oxidative stress on neuronal progenitors, where nestin positive cells were more resistant to oxidative stress driven by H_2O_2-induced apoptosis[56].

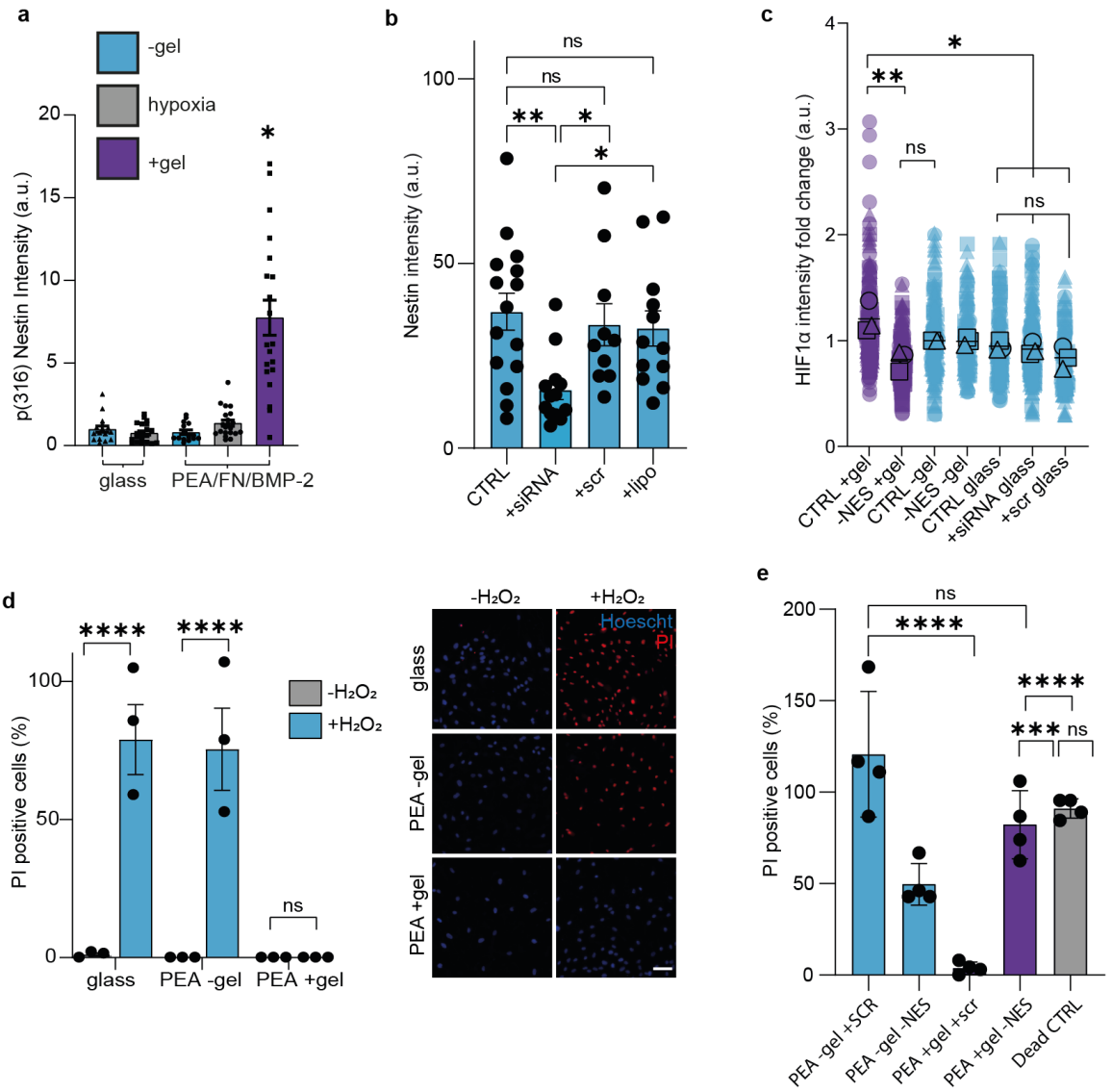

Figure 5 | Nestin is cytoprotective. a, Immunofluorescent detection of *nestin phosphorylation at Th(316) indicates it is not incorporated into intermediate filament networks, but is instead soluble. Graph is mean ±SEM, each point represents 1ximage field/number nuclei, n= 4 material replicates.* ***b****, siRNA knock-down of nestin in PerSCs was confirmed using immunofluorescence, n= 3 material replicates, graph shows mean ±SEM.* ***c****, siRNA knock-down of nestin leads to the loss of activated HIF1α co-localisation to PerSC nuclei in +gel niches; no effect on HIF1α localisation was observed in hypoxia or -gel models (where PerSCs were nestin$^{low/negative}$). N= 4 material replicates from 3 independent experiments with different donor cells. Scr = scrambled siRNA (control), lipo = lipofectamine only (control).* ***d,*** *Nestin protects from oxidative stress. PerSCs in the bioengineered models were treated with H_2O_2 to mimic oxidative stress. N= 3 material replicates, representative images shown, scale bar is 100 µm.* ***e,*** *siRNA knock-down of nestin in PerSCs and susceptibility to oxidative stress was assessed. In the +gel niches, nestin knockdown led to similar levels of cell death as in the -gel niches (nestin$^{low/negative}$ systems). All conditions were +H_2O_2, dead CTRL +10 mM H_2O_2. N= 4 material replicates. D and e measured by the % of propidium iodide (PI) positive cells vs total Hoechst stained nuclei. Statistics by one-way ANOVA with Tukey multiple comparisons *p< 0.05, **p<0.005, ***p<0.0005, **** p< 0.0001, ns = non-significant.*

Engineered Niches Maintain LT-HSCs ex vivo.

Next, we investigated whether our bioengineered niches could maintain LT-HSCs. Typically, HSC expansion media contains a cocktail of GFs. Here, we used a defined basic media (0% HSC Media; see Methods), which we supplemented with three necessary GFs (Flt3L (FMS like

tyrosine kinase 3 ligand, 50 ng/mL); SCF (20 ng/mL); and TPO (25 ng/mL)) to make a standardised HSC media (called 100% HSC media). When HSCs were cultured in 100% media in standard tissue culture well plates, we refer to it as the 'gold standard' condition.
To test the niche conditions on maintenance of the $CD34^{+ve}/CD38^{-ve}$ HSC population, PerSCs were first cultured in the bioengineered models for 14 days in stromal cell media (see Methods). $CD34^{+ve}$ HSCs from human bone marrow were then added to the niches when the media was changed to either 0% HSC media, or 100% HSC media. The cells were co-cultured for a further 5 days (Figure 6a), and then released with collagenase for flow cytometry analysis. Our strategy (as shown in Figure 6b) excluded PerSCs from this analysis, by gating on CD45 positive cells and then defining and quantifying the $CD34^{+ve}/CD38^{-ve}$ population. This population is commonly referred to as HSCs, but, in fact, contains both LT and ST-HSC populations. Gold-standard culture conditions showed a 6-fold increase in $CD34^{+ve}/CD38^{-ve}$ cell numbers after 5 days of culture in the bioengineered models (Figure 6c). When $CD34^{+ve}$ HSCs were co-cultured with PerSCs in -gel models, they expanded to a similar extent in both 0% and 100% HSC media, indicating that the PerSCs could support HSC expansion (Figure 6c). However, when $CD34^{+ve}$ HSCs were co-cultured with PerSCs in hypoxic models or in the +gel niches, no expansion was observed in the $CD34^{+ve}/CD38^{-ve}$ population (Figure 6c).

As previously noted, LT-HSCs are inherently quiescent, making the expansion of this population, without differentiation, difficult[4]. Thus, strategies that robustly maintain LT-HSC functional properties in vitro are still unresolved. We therefore investigated if our bioengineered niches could maintain LT-HSC numbers rather than just a $CD34^{+ve}/CD38^{-ve}$ heterogenous population. To enumerate LT-HSCs, long-term culture-initiating cell (LTC-IC) assays were performed to identify the number of naïve LT-HSCs within a $CD34^{+}$ mixed population. In this assay, defined culture conditions (feeder layers and media) are used in which ST-HSCs and progenitors die over 6 weeks. The potency of the remaining LT-HSCs was then tested using a colony forming unit assay (CFUs), in which the differentiation potential of individual LT-HSCs were tested in methylcellulose cultures for a further 7 days.

BM $CD34^{+ve}$ cells were co-cultured in engineered niches, and subsequently FACS sorted for $CD45^{+ve}/Lin^{-ve}/CD34^{+ve}$ markers to remove committed progenitors and PerSCs (supplementary Figure 5a). In the -gel condition with 0% or 100% HSC media, increased numbers of $CD34^{+ve}/CD38^{-ve}$ HSCs were observed compared to the starting population (i.e. expansion) (Figure 6c); however, fewer LT-HSCs were preserved compared to the gold-standard conditions (Figure 6d). In the +gel niches with 100% HSC media, no $CD34^{+ve}/CD38^{-ve}$ expansion was noted (Figure 6c) and LT-HSC numbers were reduced demonstrating phenotypic drift (Figure 6d). Importantly, the +gel niche with 0% HSC media maintained both total $CD34^{+ve}/CD38^{-ve}$ cell numbers (Figure 6c) and there was an increase in LTC-IC numbers as shown by an increase in CFUs (Figure 6d). This indicates that the $CD34^{+ve}/CD38^{-ve}$ expansion observed in the gold standard condition must have been in the ST-HSC/progenitor population as it did not lead to an increased number of LT-HSCs compared to +gel 0% (Figure 6c & d). It is noteworthy that the subsequent differentiation profile of LT-HSCs from the +gel niche with 0% HSC media mimics that of the gold standard cultures, with no loss of lineage commitment, as indicated by the ability to reconstitute all blood cell progenitors (Figure 6e, supplementary Figure 5b).

To demonstrate the therapeutic potential of our engineered niches, we also investigated their ability to support CRISPR edited HSCs. The cellular repair of CRISPR-mediated double-strand DNA breaks in dividing cells primarily occurs via canonical non-homologous end-joining (C-NHEJ) or alternative end-joining processes like microhomology-mediated end-joining (MMEJ). It has previously been shown that quiescent LT-HSCs can be CRISPR edited primarily via C-NHEJ, while retaining engraftment potential[59]. As a proof of concept, we targeted the neutral AAVS1 (*PPP1R12C* intron 1) locus (Figure 6f), which can be edited in HSCs without loss of phenotype[59]. Using a NHEJ CRISPR strategy, we transfected primary human CD34^{+ve} BM cells with ribonuclear protein (RNP) complexes of Cas9 and AAVS1_A1 single guide RNA (sgRNA) and seeded the cells into our bioengineered niches immediately after transfection. We then assessed if the different niche microenvironments could improve the survival of CRISPR edited cells by assessing the fractions of edited HSCs after standard culture, or in the -gel and +gel niches, with either 100% or 0% HSC media. As expected, mutagenesis levels were low in these primary human HSCs. We achieved just ~5-6% mutagenesis in 100% HSC media (~2% in 0% HSC media) in both standard and -gel conditions (Figure 6g). However, notably higher levels of CRISPR edited HSCs were retained in the +gel niche, in both 100% and 0% HSC media conditions at ~10% and ~9% respectively (Figure 6g).

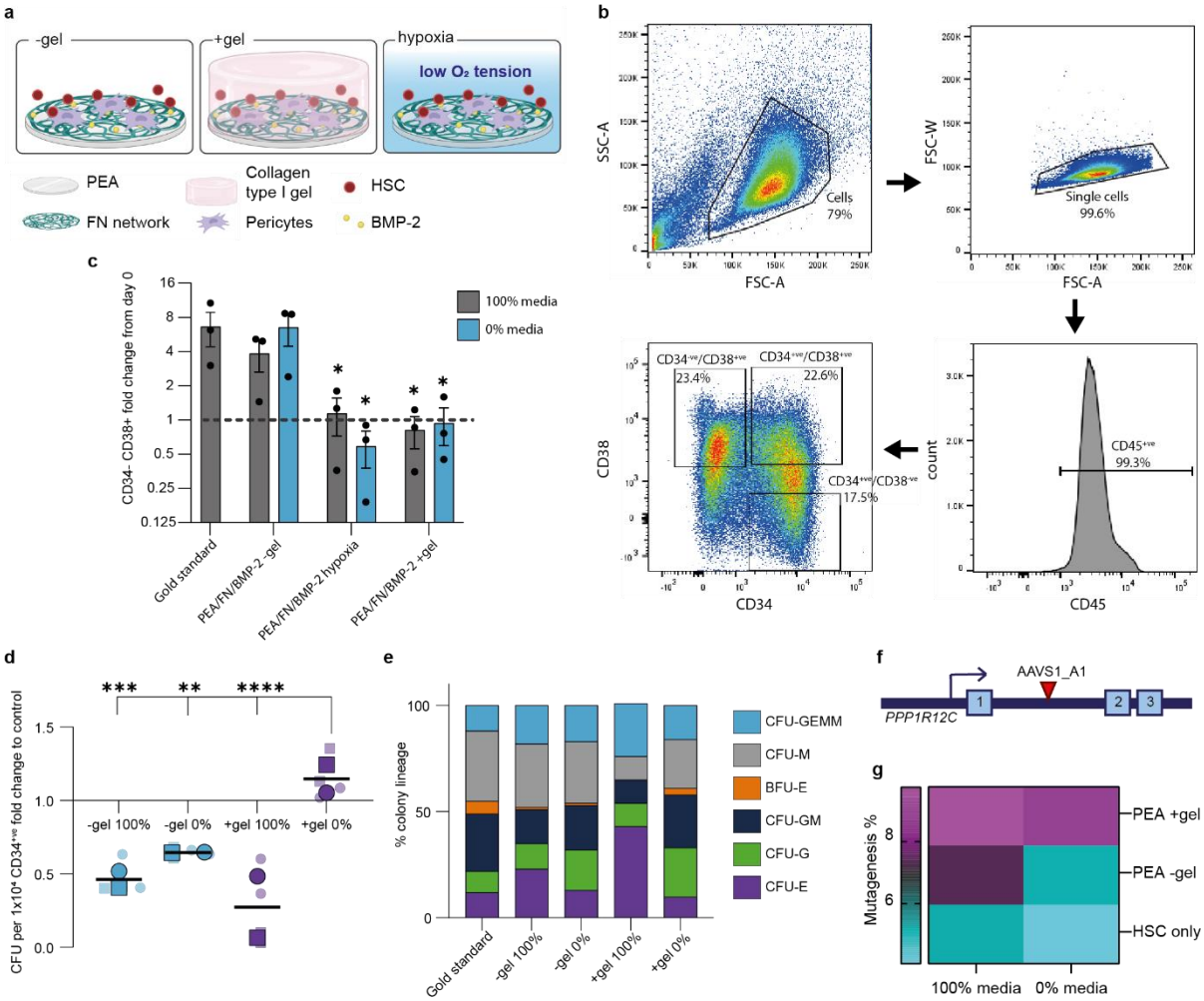

Figure 6| Engineered niches support LT-HSC maintenance and CRISPR editing. ***a***, *Schematic of the experimental set up.* ***b***, *Representative gating strategy used for HSC identification. Forward (FSC-A) versus side scatter area (SSC-A) plots were used to identify viable cells; FSC-A versus FSC width (FSC-W) plots were used to identify single cells. A gate was added on CD45^{+ve} cells to exclude any PerSCs and 3 gates were used to identify CD34^{+ve}/CD38^{--}*

^{ve}, CD34^{+ve}/CD38^{+ve} and CD34^{-ve}/CD38^{+ve} populations. The CD34^{+ve}/CD34^{-ve} population represents both LT- and ST-HSCs, whereas the CD34^{+ve}/CD38^{+ve} and CD34^{-ve}/CD38^{+ve}populations represent haematopoietic stem and progenitor cells and committed progenitors, respectively. ***c****, Fold change in CD34^{+ve}/CD38^{-ve} cell number after 5 days of culture in 100% or 0% HSC media relative to the number at day 0. Each data point = 1 donor cell line from 3 independent experiments (with 6 pooled material replicates/donor).* ***d****, Total number of colonies maintained in the bioengineered models. CD34^{+ve} cells were harvested from niche models after 5 days co-culture in 0% or 100% HSC media. Sorted CD34^{+ve} cells were then added to LTC-IC assays for 6 weeks, and the resulting cells assessed using a CFU differential assay. Total colony numbers were counted and are represented as CFUs per 1 x 10^4 CD34^{+ve} cells as fold change to control = 'gold standard', HSC only in 100% media without PerSCs. Statistics by one-way ANOVA with Tukey multiple comparisons, *p< 0.05, **p<0.005, ***p<0.0005, **** p< 0.0001. , cells from 2 donors (donor 1 = circles, donor 2 = squares).* ***e****, Lineage specification state of CFUs from bioengineered models were identified and enumerated; Colony forming unit (CFU) -granulocyte, erythrocyte, macrophage, megakaryocyte (-GEMM), -macrophage (-M), -granulocyte, macrophage (-GM), -granulocyte (-G), -erythroid (-E), burst forming unit -erythroid (BFU-E).* ***f****, Schematic showing the AAVS1_A1 CRISPR target site at the PPP1R12C gene locus.* ***g****, Increased retention of AAVS1 CRISPR edited HSCs following culture in the +gel niches with 100% or 0% media, relative to culture in gold standard or -gel conditions. The heatmap shows the level of % AAVS1 mutagenesis, n = 2 donors, 3 pooled material replicates.*

Discussion

In this study we set out to show that a combination of materials could be used to organise the ECM, GF presentation and elastic environment of a putative BM niche. In vivo, the BM endosteum is densely perfused with a network of thin-walled arterioles[13,25]. These arterioles are closely associated with nestin^{+ve} PerSCs[12,13,18], and HSCs isolated from this area show greater engraftment potential than their central marrow (sinusoidal) counterparts[60]. Here, we report a first attempt to bioengineer this endosteal/arteriolar region of the BM niche, by promoting a niche-like phenotype in PerSCs that can support and maintain LT-HSCs, the HSC population that resembles those isolated from this niche region in vivo.

The +gel niche model developed here supports the expression of nestin in PerSCs, a phenotype that has been well-reported to be critical for the stromal-HSC supportive phenotype in vivo[12,13,18,28] and has been shown to have increased expression in stromal cells in soft environments[19]. Indeed, expression of nestin by PerSCs correlates with increased expression of other important niche factors, such as HSC maintaining cytokines, decreased oxidative phosphorylation/respiration[38,61], and increased cytoprotection[54–56]. We demonstrate that nestin-linked changes in PerSC respiration were central to the LT-HSC supportive phenotype. Nestin was further implicated in the persistent expression of nuclear HIF1α in the absence of low oxygen tension and without changes in the expression of hypoxia-signalling targets. This has parallels to cancer cells using HIF metabolism without hypoxia in the Warburg effect[53].

This new approach towards LT-HSC maintenance is important, as most studies focus on expansion of the total heterogenous HSC population in vitro, and do not separate naïve LT-HSCs from other committed progenitor populations[10,29,31]. Currently, expansion of LT-HSCs and the mechanisms required remain elusive. It is likely that clinically relevant expansions (e.g. 1 donor to multiple recipients) will require genetic manipulations/perturbation as naturally quiescent LT-HSCs will be required to enter the cell cycle and proliferate, then return to the resting state[62]. Until these fundamental principles of LT-HSC dynamics are understood and can be harnessed, systems that focus on their effective maintenance are required to help understand these dynamics and to improve therapeutic applications such as drug development, alloSCT or gene editing.

Here, our data suggests that the use of common exogenous GF supplementation in combination with these niche co-cultures provides excessive stimulation to the HSC population and results in the loss of quiescence. However, by manipulating microenvironments to tune stromal cell physiology, LT-HSCs can be maintained in vitro without any exogenous supplementation. The CFU data (Figure 6d) indicates that the $CD34^{+ve}/CD38^{-ve}$ expansion (Figure 6c) observed in the gold standard condition must have been in the ST-HSC/progenitor population, as it did not lead to an increase in the number of CFUs (i.e. LT-HSCs), in fact, CFUs decreased compared to culture in the +gel niche. As such, we suggest that the use of the optimised +gel niche avoids the unwanted ST-HSC/progenitor expansion that comes with the concomitant sacrifice of LT-HSC numbers.

Furthermore, once we had established a LT-HSC maintenance niche and investigated a role for nestin in PerSC support phenotype, we went on to investigate a potential use for the niches in supporting CRISPR editing. Using a NHEJ-based CRISPR approach that facilitates the targeting of quiescent cells, such as LT-HSCs[59], we demonstrated that our bioengineered niches improve the survival of CRISPR edited HSCs. This is important because of the very low abundance of LT-HSCs and shows that our niches can maintain these cells. For such approaches to be used successfully to gene edit HSCs for therapeutic purposes, CRISPR editing rates in LT-HSCs, and LT-HSC survival, will need to be as high as possible to ensure that enough of the edited population can engraft and rebuild the blood system.

Our study has limitations in that it uses a natural hydrogel, collagen. Changing to use of a synthetic hydrogel would have advantages in increased reproducibility/control of viscoelasticity, degradability and biological milieu[63]. Further, while we advocate an approach of LT-HSC maintenance, the ability to robustly expand this population is deeply alluring. In the BM niche, the LT-HSCs are produced or, perhaps, dedifferentiated from ST-HSCs/progenitor cells[62]. Looking to bioengineer the sinusoidal niche, with different ECM constiuents[39,40], different stromal support[13] and different oxygen tension[25], could thus be interesting and rewarding.

Acknowledgements

We thank Dr Gillian Higgins for provision of adipose tissue to isolate PerSCs and Dr Mark Sprott for help with ethyl acrylate synthesis. We thank Carol-Anne Smith for technical assistance. We also thank the University of Glasgow Polyomics Facility, particularly Dr Karl Burgess and Dr Gavin Blackburn. This work was supported by BBSRC grant BB/N018419/1, EPSRC grant EP/P001114/1, MRC grant MR/R005567/1 and the Carnegie Trust grant number RIG009892.

Methods

Preparation of materials and ECM interfaces

Polymer sheets were obtained by radical polymerization of a solution of either MA (methyl acrylate) or EA (ethyl acrylate) (Sigma-Aldrich, UK), using 1 and 0.35 weight percent benzoin (98% pure; Scharlau) as the photoinitiator. Polymerization carried out up to limiting conversion. After polymerization, low molecular mass substances extracted by drying under vacuum to constant weight. PMA and PEA were dissolved in toluene at a concentration of 6%

or 9% and 2.5% or 12% dependent on batch. Spin casting was performed on glass coverslips at 2000 rpm for 30 s. Samples dried under vacuum at 60°C for 2 h, and sterilised under UV light for 30 min before use[35]. FN from human plasma (Sigma-Aldrich, F2006) was adsorbed from solutions of 20 µg/ml for 1 h a room temperature (RT) then washed thrice with phosphate-buffered saline (PBS). For GF adsorption, BMP-2 (50 ng/ml,; Sigma-Aldrich, H4791) in PBS was used for 2 h at RT. Finally, samples were rinsed in PBS to eliminate non-adsorbed protein.

Atomic force microscopy

FN was prepared in PBS (20 µg/ml) and a 200 µl droplet placed on surface of PEA and PMA coated coverslips. The protein was adsorbed for 10 min and remaining liquid removed from the surface. Surfaces were then washed twice in PBS, once with deionised water and then dried under a stream of nitrogen before imaging. A JPK Nanowizard 4 (JPK Instruments) was used for imaging in tapping mode, using antimony-doped Si cantilevers with a nominal resonant frequency of 75 kHz (MPP-21 220, Bruker). The phase signal was set to 0 at a frequency 5-10% lower than the resonant frequency. Height and phase images were acquired from each scan, the JPK data processing software version 5 was used for image analysis.

FN adsorption assays

To quantify amount of FN adsorbed onto PEA or PMA surfaces substrates were coated with 20 µg/ml FN/PBS solution for 1 h, aspirate was collected and FN quantified using the Pierce™ BCA Protein Assay Kit (Thermo Fisher, UK). Quantitative immunofluorescence assays were carried out using the LI-COR in-cell western™ platform. FN (20 µg/ml) was adorbed as previously described, samples were washed with PBS, blocked with 1% milk protein in PBS, and incubated with primary antibodies for total FN (polyclonal rabbit, Sigma Aldrich), HFN7.1 (monoclonal mouse, Developmental Studies Hybridoma Bank, USA), and P5F3 (monoclonal mouse, Santa Cruz Biotechnology, sc-18827) for 2 h. Substrates were washed 5x 0.5% Tween20 in PBS (PBST), followed by incubation o/n at 4ºC with LI-COR secondary antibodies (IRDye 800CW/700CW anti-rabbit/mouse secondary antibody, LI-COR, UK). Samples were washed 5x with PBST, followed by a final wash in PBS and dried before imaging on LI-COR Sa Odyssey scanner.

BMP-2 adsorption

For quantification of BMP-2 adsorption, (50 ng/ml) BMP-2 solution was added to FN coated polymers and after 2 h incubation solution was aspirated and collected in Protein LoBind Tubes (Eppendorf™). Enzyme-linked immunosorbent assays (ELISA) was then carried out as per manufacturer's instructions (R&D Systems, BMP-2 DuoSet ELISA kit, DY355). Briefly, ELISA plates were coated with capture antibody overnight, then blocked for 1 h with BSA. Standards, original solution, original solution at 20x dilution and sample aspirates were then added to the plate, and bound BMP-2 was detected with biotinylated anti-human BMP-2. Streptavidin-HRP was added to plates for 20 min in the dark, followed by substrate solution (tetramethylbenzidine and peroxide) for 20 min, the reaction was then stopped by adding stop solution. Absorbance measured at 450 nm with wavelength correction at 570 nm.

PerSC isolation

PerSCs were isolated from the adipose tissue of healthy adult donors undergoing cosmetic lipectomy procedures with prior written consent, or from patients undergoing breast

reconstruction procedure, using deep inferior epigastric perforators (DIEP), from adult donors. Ethical approval for the collection of tissue and subsequent research was granted by the South-East Scotland Research Ethics Committee 3 (SESREC03, reference no. 10/S1103/45). Incisions were made in the adipose tissue using a scalpel to divide the Scarpa's fascial layer, then tissue was mechanically disrupted, combined with PBS and centrifuged at 445 g for 10 mins at RT, causing phase separation. The 3 phases include the top phase (liquid fat/oil), central phase containing the tissue of interest (adipose tissue), and the bottom phase (blood/fluid). Middle layer was removed and mixed with equal volumes of PBS/2% (v/v) fetal bovine serum (FBS) and centrifuged at 445 g for 10 mins. Supernatant was discarded and the remaining Stromal Vascular Fraction (SVF) pellet, was enzymatically digested with type II-S collagenase 1 mg/ml in DMEM/0.5% (v/v) BSA for 45 mins at 37°C. Samples were centrifuged and supernatant discarded (containing oil and adipocytes) and pellets resuspended and strained through 400 µm, 100 µm and 70 µm cell pluristrainers to remove undigested material. Red blood cell lysis buffer was added to eliminate erythroid cells and SVF pellet resuspended in Fluorescent Activated Cell Sorting (FACS) buffer. Cells sorted on $CD146^{+ve}/CD45^{-ve}/CD34^{-ve}/CD31^{-ve}$ phenotype (anti-CD146 clone P1H12, BV711, 563186; anti-CD45 clone H130, V450, 560367; anti-CD34 clone 581, FITC, 555821; anti-CD31 clone WM59, PE-Cy7, 563651. All BD Biosciences), using BD FACSAria cell sorter (BD Biosciences). Immediately after sorting, cells were then cultured as previously described[16]. Briefly, cells were cultured in endothelial growth medium (EGM-2, Lonza) on 0.1% gelatin-coated plates in a humidified incubator with 5% CO_2 at 37°C until passage 1.

Cell culture

PerSCs, after passage 1, were cultured in Dulbecco's Modified Eagle's Medium (DMEM, Sigma-Aldrich) with 20% FBS (Thermo Fisher), 1% nonessential amino acids (Sigma-Aldrich), 1% 100 mM sodium pyruvate (Sigma-Aldrich) and an antibiotic mix consisting of 10 mg/ml penicillin/streptavidin (Sigma-Aldrich), 200 nM L-glutamate (Sigma-Aldrich), and 0.5% Fungizone (Thermo Fisher). Cells were incubated in a 5% humidified CO_2 atmosphere at 37°C. For cell culture on polymer substrates, cells were seeded at 1.5 $x10^3/cm^2$ on 13 mm coverslips in 24 well-plates and cultured in DMEM containing 2% with human AB serum (HS; Sigma Aldrich, H4522) in a 5% humidified CO_2 atmosphere at 37°C. Hypoxic culture carried out in hypoxic workstation (Ruskinn) at an oxygen tension of 1%, CO_2 5% and 37°C. Medium was exchanged every 3 days. $CD34^{+ve}$ cells from human BM were purchased from CalTag Medystems (experiments related to Figure 6b-e) and STEMCELL Technologies (Figure 6f). $CD34^{+ve}$ cells were cultured in serum free medium; Iscove's Modified Dulbecco Medium (IMDM) containing 20% BIT 9500 serum substitute (STEMCELL Technologies), 1% 200 mM L-glutamine (Sigma-Aldrich), 1% 10 mg/ml penicillin/streptomycin (Invitrogen) supplemented with Flt3L (50 ng/ml), SCF (20 ng/ml) and TPO (25 ng/ml) (all recombinant human, Peprotech, 300-19, 300-07, 300-18) (100% medium). $CD34^{+ve}$ cells were thawed, counted and rested overnight in 100% medium at a density of $0.5x10^6$/ml, then recounted, suspended in 100% or 0% media, and seeded into niche models at a density of $5x10^4$ cells/ml, with 0.5 ml added to each well of 24 well plate. For conditions containing gels, the HSCs were seeded on top of the gel. Control (100% media only) were seeded into 24 well-plates. Seeded cells were then cultured for 5 days. At least $1x10^3$ cells were transferred to an Eppendorf tube and phenotyped at day 0 using flow cytometry.

Collagen gel preparation and rheological measurement

Collagen type I gels were added to relevant (+gel) conditions after either 24h (for short term culture) or 72h (for long term culture). Rat tail collagen type I solution in 0.6% acetic acid (First Link, UK) was combined with human AB serum (HS; Sigma-Aldrich, H4522), 10x DMEM, 2% HS DMEM, adjusted to pH 8.2 using 0.1 M NaOH. 1 ml of solution was then added to 24 well-plates containing PEA coated 13 mm coverslips. Resulting gels were ~1 cm thick. Rheological measurements were carried out using an Anton Paar Physical MCR301 rheometer. A parallel plate geometry (25 mm diameter, sandblasted) and 1.0 mm gap were used to measure time sweeps. The dynamic modulus of the hydrogel was measured as a frequency function, with frequency sweeps carried out between 0.1 – 15 Hz to measure the dynamic shear of the modulus as a function of strain. Measurements were repeated 3 times on gels from 3 different batches. Storage moduli (G´) values were extracted from the accompanying Kinexus software. The Young's modulus was then determined by taking the G´ and multiplying by 3, assuming a Poisson's ratio of 0.5 in accordance with Hooke's law.

Immunocytochemistry

PerSCs were cultured in niches for times indicated and fixed using 10% formaldehyde for 15 mins. For SCF and CXCL12 analysis, cells were cultured with 5 µg/ml brefelndin A (Sigma-Aldrich, B6542), for the final 24h of culture before fixation. Cells were then permealized with 0.5% Triton-X for 5 mins and blocked using 0.5% BSA/PBS for 2 h at RT. Primary antibodies were then added in blocking buffer: anti-nestin [10C2] 1:200 (mouse monoclonal, Abcam, ab22035); anti-p(Th316)-nestin [a-4] at 1:200 (mouse monoclonal, Santa Cruz Biotechnology, sc-377538); anti-HIF1α [EP1215Y] 1:300 (rabbit monoclonal, Abcam, ab51608); anti-vimentin [SP20] 1:300 (rabbit monoclonal, Thermo Fischer, MA5-16409); anti-CXCL12 1:200 (monoclonal mouse, R & D Systems, MAB350); anti-SCF 1:200 (rabbit polyclonal, Abcam, ab64677). Cells were then washed 5 x 5 mins with PBST and biotinylated secondary antibodies (1:50; Vector Laboratories) were added in blocking buffer for 2h at RT. Cells were again washed 3 x 5 mins in PBST and incubated with fluorescein isothiocyanate-conjugated streptavidin (1:50; Vector Laboratories) in blocking buffer for 30 mins at RT. Nuclei were stained using VECTASHIELD mountant with 5',6-diamidino-2-phenylindole nuclear stain (DAPI; Vector Laboratories). Samples were then mounted onto glass slides and visualised using an Axiophot microscope or Evos Cell imaging system (Thermo Fischer) and analysed using ImageJ software (National Institute of Health). HIF1α nuclear co-localisation was analysed using a custom developed pipeline on CellProfiler software (version 2.1.1).

Flow cytometry

To phenotype PerSCs and HSCs after culture, cells were harvested from niche systems using collagenase D (2.5 mg/mL in PBS; Sigma-Aldrich) and TripLE™ (Thermo Fisher). Cells were passed through a 70 µm filter, and stained on ice for 30 mins, using antibodies outlined in Supplementary Table 4 and 5 for PerSC and HSC markers, in flow cytometry buffer (PBS supplemented with 0.5% BSA and 0.5 mM EDTA). Cells were then washed twice with PBS and analysed using an BD FACSCanto ll (BD Biosciences). The BD FACSAria Cell sorter was used for $CD34^{+ve}$ sorting for LTC-IC assays. The gating strategy is shown in supplementary Figure 4. Flow cytometry files were analysed using FlowJo software (version 10.5.3, FlowJo LLC, USA).

RNA-seq

Sequencing libraries then prepared from total RNA using the Illumina TruSeq Stranded mRNA Sample Preparation Kit. Libraries were sequenced in 75 base, paired end mode on the Illumina NextSeq 500 platform. Raw sequence reads were trimmed for contaminating sequence adapters and poor quality bases using the program Cutadapt[64]. Bases with an average Phred score lower than 15 were trimmed. Reads that were trimmed to less than 54 bases were discarded. The quality of the reads were checked using the FastQC program (http://www.bioinformatics.babraham.ac.uk/projects/fastqc/) before and after trimming. The reads were "pseudo aligned" to the transcriptome using the program Kallisto[65]. The differential expression for the analysis groups were assessed using the Bioconductor package DESeq2[66]. This was provided as a service by Glasgow Polyomics Facility. One hypoxic sample failed RNA quality control. Heatmaps in Figure 2g & h were subsequently generated using Cluster 3.0 and Java Treeview 3.0 software, with average linkage clustering method. To assess expression of transcripts related to an immunomodulatory phenotype, the distribution of reads across genomic features was quantified using the R package Genomic Ranges from Bioconductor Version 3.065. Differentially expressed genes were identified using the R package edgeR from Bioconductor Version 3.066. For Figure 3a-c and supplementary Figure 2, analyses were performed within the R statistical computing framework using packages from BioConductor. Feature counts were utilized to quantify reading counts. Human ENSEMBL gene ID to gene symbol conversion was performed in BioTools (https://www.biotools.fr). The DEseq2 BioConductor package was used for outlier detection, normalisation and differential gene expression analyses. Genes passing a threshold of adjusted p-value <0.05 and a log2 fold change > 1 were considered as differentially expressed. The names of differentially expressed genes along with their respective log2fold changes were inputted into PathfindR package. Gene Ontology (GO) enrichment was conducted with PathfindR. Only pathways with FDR < = 0.05 were considered as differentially enriched. The differentially expressed genes involved in every pathway were extracted and their z-scored fold changes in expression were presented as heatmaps.

In-cell western assay for LDH

PerSCs were cultured in niches for 7 days then fixed using 10% formaldehyde for 15 min. The cells were then permealized with 0.5% Triton-X for 5 mins and blocked using 0.5% milk protein in 1X PBS. Anti-lactate dehydrogenase (LDH) [EP1566Y] (rabbit monoclonal, Abcam, ab52488) was added at 1:200 in 0.5% milk PBS and incubated at 4°C overnight, followed by 5 washes in PBST. CellTag 700 stain (LI-COR, 926-41090) was used as the reference control, and was added with LI-COR anti-rabbit secondary antibody (926-32211), at 1:2000 in 0.5% milk PBST and incubated at RT on a shaker for 2 h, followed by 5 x 5 min washes with PBST. The quantitative spectroscopic analysis was the carred out using the LI-COR Odyssey Sa.

VEGF ELISA

PerSCs were cultures in niche systems and media supernatant was collected in Protein LoBind Tubes (Eppendorf™) at day 7 and 14 and stored at -20°C. ELISA for VEGF was then carried out as per manufacturer's instructions (R&D Systems, VEGF Quantikine ELISA kit, DVE00). Standards and media aspirate were added to the ELISA plate in duplicate. Absorbance measured at 450 nm with wavelength correction at 570 nm.

Hypoxyprobe™ assay

PerSCs were cultured in niche models for 6 days, medium was then changed to fresh medium containing 200 µM pimonidazole (Hypoxyprobe™, HP1-200kit), and cultured for a further 24h. Cells were then fixed, permealised and blocked as described for immunocytochemistry. Mouse monoclonal anti-pimonidazole (1:200; Hypoxyprobe™, HP1-200kit) was added in blocking buffer and incubated overnight at 4°C. Cells were washed 3 x 5 mins in PBST and incubated with anti-mouse secondary (1:50, Texas Red; Vector Laboratories) for 2 h at RT. Cells were washed 3 x 5 mins in PBST and mounted onto glass slides with DAPI nuclei stain VECTASHIELD mountant(Vector Laboratories). Samples were visualised on Evos Cell imaging system (Thermo Fischer) and analysed using ImageJ software (National Institute of Health).

Lactate assay

PerSCs were cultured in niche systems in DMEM with 2% dialyzed FBS (Thermo Fischer, A3382001), cell media supernatant was aspirated at 7 and 14 days and stored at -20°C. Lactate levels in supernatant were then measured using the Lactate-Glo™ assay (Promega, J5021) as per manufacturers protocol. Briefly, samples were diluted 1:100 and mixed 1:1 with Lactate Detection Reagent in 96-well plate and incubated for 1 h at RT. Luminescence was read using PHERAstar FSX microplate reader (BMG Labtech).

Metabolomics

Whole cell metabolomic analysis was performed on cell lysates isolated from PerSCs cultured in niche systems for 7 or 14 days. Substrates were washed with ice-cold PBS, and cells lysed in extraction buffer (PBS/methanol/chloroform at 1:3:1 ratio) for 60 mins at 4°C with constant agitation. Lysates were then transferred to cold Eppendorfs™ and spun at 13000 g at 4°C for 5 mins to remove debris and stored at -80°C. Cleared extracts were used for hydrophilic interaction LC/MS analysis (UltiMate 3000 RSLC, (Thermo Fisher), with a 6 150 x 4.6 mm ZIC-pHILIC column running at 300 µl/min-1 and Orbitrap Exactive). A standard pipeline, consisting of XCMS (peak picking), MzMatch (filtering and grouping) and IDEOM (further filtering, post-processing and identification) was used to process the raw mass spectrometry data. Identified core metabolites were validated against a panel of unambiguous standards by mass and predicted retention time. Further putative identifications were generated by mass and predicted retention times. Heatmaps of selected metabolites and principle component analysis (PCA) plots were generated using MetaboAnalyst software (version 4.0). This was provided as a service by Glasgow Polyomics Facility.

$^{13}C_6$-Glucose metabolomic tracing

PerSCs were seeded onto PEA/FN/BMP-2 niche systems and allowed to grow for 72 h. Cells were then washed and media was changed to basal media comprising 25% normal glucose and 75% $^{13}C_6$-Glucose (Cambridge Isotopes Ltd). Extraction performed in PBS/methanol/chloroform at 1:3:1 ratio, after 3 days incubation and prepared for LC-MS. The LC-MS platform consisted of an Accela 600 HPLC system combined with an Exactive (Orbitrap) mass spectrometer (Thermo Fisher). Two complementary columns were used; the zwitterionic ZICpHILLIC column (150 mm x 4.6 mm; 3.5 µm, Merck) and the reversed phase ACE C18-AR column (150 mm x 4.6 mm; 3.5 µm Hichrom) and in both cases sample volume was 10 µl at a flow rate of 0.3 ml/min. Eluted samples were then analysed by mass spectrometry. Raw data from LC-MS of ^{13}C-labelled extracts was processed to generate a combined PeakML file[67]. Further analysis using mzMatch-ISO in R[68] generated a PDF file

containing chromatograms used to check peak-shape and retention time, and a tab delineated file detailing peak height for each isopotologue, which was used to calculate percentage labelling. Samples normalised to cell number. Total $^{13}C_6$-Glucose incorporation was calculated by totalling incorporation excluding up to C2 to eliminate natural incorporation. This was provided as a service by Glasgow Polyomics Facility.

siRNA NES silencing NES

PerSCs were seeded into niche models in antibiotic free 2% HS DMEM, after 24 h media was changed to Opti-MEM™ (Thermo Fisher) and siRNA transfection was carried out 24 h later. Pre-designed Silencer™ Select siRNA NES (ID: 21141), or Silencer™ Select negative control number 1 siRNA (both Thermo Fischer), was incubated at RT for 20 mins with Lipofectamine™ RNAiMAX (Thermo Fisher) in Opti-MEM™ and added to PerSCs in niches. 6 hours later, Opti-MEM™ +2% HS was added to control and -gel conditions. For +gel, media containing siRNA was collected and used to prepare collagen gels as described above. Once collagen had set, Opti-MEM™ +2% HS was added. Cells were then cultured for 72h and either fixed for immunofluorescence analysis or cytotoxicity assays carried out.

Cytotoxity assay

Cells were cultured in niche models for time points indicated. Collagen gels were removed and 1000 µm H_2O_2 added for the final 6 h of culture. Hoechst (33342) nuclear stain (Thermo Fischer, R37605) and Propidium Iodide (PI) (Biolegend, 421301) viability stain was then added and imaged on EVOS M7000 imaging system using the on-stage incubator.

LTC-IC assay

LTC-IC assays were carried out on sorted $CD45^{+ve}$/$Lineage^{-ve}$/$CD34^{+ve}$ cells harvested after 5 days of culture in niche systems. Engineered stromal fibroblast feeder layers were first established. M2-10B4 (overexpressing IL-3 and G-CSF) and Sl/Sl (overexpressing IL-3 and SCF) were passaged at ~90% confluence (cell lines gifted from STEMCELL Technologies). Cells were grown for 2 weeks prior to use in selection agents to select stromal cells expressing long-term cell maintenance factors (M2-10B4, 0.4mg/ml G418 and 0.06mg/ml Hygromycin B; Sl/Sl, 0.8 mg/ml G418 and 0.15 mg/ml Hygromycin B) G418 and Hyfromycin B both STEMCELL Technologies (03812, 03812). Cells at ~80% confluence were irradiated with 8000 cGy, trypsinised. M2-10B4 and Sl/Sl were mixed at 1:1 ratio at a final concentration of $1.5x10^6$/ml. Cells were then seeded into collagen coated 24 well plates (Thermo Fisher, A1142802) for 24 hours before adding sorted cells. Cultures were then maintained for 6 weeks in MyeloCult™ (STEMCELL Technologies, 05150) supplemented with $1x10^{-6}$ M hydrocortisone (StemCell Technologies, 74142), with half media exchanges twice per week.

CFU Assay

Cells were harvested and resuspended in MethoCult™ (STEMCELL Technologies, 04435) from LTC-IC assays after 6 weeks. 2 replicates were seeded for each condition in 35 mm dishes and incubated at 37°C in 5% CO_2 for 5 days. After 7 days total colonies were counted and phenotyped using a light microscope.

CRISPR

$CD34^{+ve}$ cells were thawed 24 h before electroporation and cultured in IMDM +BIT +100% cytokine media without antibiotics. Ribonucleoprotein (RNP) complexes were prepared by

mixing Cas9 (IDT) at 12 µM and AAVS1_A1 sgRNA (GTCACCAATCCTGTCCCTAG, Synthego) at 12 µM, in electroporation buffer R (Thermo Fisher) with 2% glycerol[59], and incubated for 15 min at RT immediately before electroporation. Electroporation was performed using the Neon™ transfection system, with 10 µl tips (Thermo Fisher), as per manufacturers protocol. The optimal electroporation conditions for $CD34^{+ve}$ cells was 1700 V, 20 ms, one pulse. $CD34^{+ve}$ cells were resuspended in buffer R and mixed with assembled RNPs. Electroporated cells were resuspended in either 100% or 0% cytokine IMDM +BIT and 0.5 ml added into niche models at a density of $5x10^4$ cells/ml. Cells were then cultured for 5 days, and harvested as previously described using collagenase D, with final resuspension into 30 µl of Quick Extract™ reagent (Lucigen). For mutagenesis analysis, Quick Extract samples were diluted 1:1 with fresh QuickExtract and heated to 65 °C for 6 mins, vortexed for 15 s, and heated to 98 °C for 2 mins. Genomic PCR was carried out using Herculase II Fusion DNA Polymerase (Agilent) (Forward primer: CCCCGTTCTCCTGTGGATTC, Reverse primer: ATCCTCTCTGGCTCCATCGT). PCR products were run on 1.2 % UltraPure™ Agarose (Invitrogen) gels, purified (QIAquickPCR Purification Kit, Qiagen) and Sanger Sequenced (Eurofins Genomics). Mutagenesis analysis was carried out by TIDE analysis[69] (http://shinyapps.datacurators.nl/tide/) (supplementary figure 5).

Data availability

Raw data is available at http://dx.doi.org/10.5525/gla.researchdata.1326.

References

1. Burns, R., Leal, J., Sullivan, R. & Luengo-Fernandez, R. Economic burden of malignant blood disorders across Europe: a population-based cost analysis. *Lancet Haematol.* **3**, e362–e370 (2016).
2. Granot, N. & Storb, R. History of hematopoietic cell transplantation: Challenges and progress. *Haematologica* **105**, 2716–2729 (2020).
3. Registry, T. A. N. and N. S. C. State of the Registry 2020-2021. 1–10 (2022).
4. Zon, L. I. Intrinsic and extrinsic control of haematopoietic stem-cell self-renewal. *Nature* **453**, 306–313 (2008).
5. Yang, L. *et al.* Identification of Lin-Sca1+kit+CD34 +Flt3- short-term hematopoietic stem cells capable of rapidly reconstituting and rescuing myeloablated transplant recipients. *Blood* **105**, 2717–2723 (2005).
6. Dexter, T. ., Moore, M. A. . & Sheridan, A. P. . Maintenance of hemopoietic stem cells and production of differentiated progeny in allogeneic and semiallogeneic bone marrow chimeras in vitro. *J. Exp. Med.* **145**, 1612–1616 (1977).
7. Nakauchi, H., Sudo, K. & Hideo, E. M. A. Quantitative assessment of the stem cell self-renewal capacity. *Ann. N. Y. Acad. Sci.* **938**, 18–25 (2001).
8. Li, J. *et al.* Development and clinical advancement of small molecules for ex vivo expansion of hematopoietic stem cell. *Acta Pharm. Sin. B* **12**, 2808–2831 (2021).
9. Fares, I. *et al.* EPCR expression marks UM171-expanded CD34+ cord blood stem cells. *Blood* **129**, 3344–3351 (2017).
10. Wagner, J. E. *et al.* Phase I/II Trial of StemRegenin-1 Expanded Umbilical Cord Blood Hematopoietic Stem Cells Supports Testing as a Stand-Alone Graft. *Cell Stem Cell* **18**, 144–155 (2016).
11. Pinho, S. & Frenette, P. S. Haematopoietic stem cell activity and interactions with the

niche. *Nat. Rev. Mol. Cell Biol.* (2019) doi:10.1038/s41580-019-0103-9.
12. Méndez-Ferrer, S. *et al.* Mesenchymal and haematopoietic stem cells form a unique bone marrow niche. *Nature* **466**, 829–834 (2010).
13. Kunisaki, Y. *et al.* Arteriolar niches maintain haematopoietic stem cell quiescence. *Nature* **502**, 637–643 (2013).
14. Ding, L. & Morrison, S. J. Haematopoietic stem cells and early lymphoid progenitors occupy distinct bone marrow niches. *Nature* **495**, 231–235 (2013).
15. Sacchetti, B. *et al.* Self-Renewing Osteoprogenitors in Bone Marrow Sinusoids Can Organize a Hematopoietic Microenvironment. *Cell* **131**, 324–336 (2007).
16. Crisan, M. *et al.* A Perivascular Origin for Mesenchymal Stem Cells in Multiple Human Organs. *Cell Stem Cell* **3**, 301–313 (2008).
17. Sugiyama, T., Kohara, H., Noda, M. & Nagasawa, T. Maintenance of the Hematopoietic Stem Cell Pool by CXCL12-CXCR4 Chemokine Signaling in Bone Marrow Stromal Cell Niches. *Immunity* **25**, 977–988 (2006).
18. Pinho, S. *et al.* PDGFR A and CD51 mark human stem cells capable of hematopoietic progenitor cell expansion. *J. Exp. Med.* **210**, 1351–1367 (2013).
19. Engler, A. J., Sen, S., Sweeney, H. L. & Discher, D. E. Matrix elasticity directs stem cell lineage specification. *Cell* **126**, 677–89 (2006).
20. Klamer, S. & Voermans, C. The role of novel and known extracellular matrix and adhesion molecules in the homeostatic and regenerative bone marrow microenvironment. *Cell Adhes. Migr.* **8**, 563–577 (2014).
21. Chen, X. *et al.* Mechanical Heterogeneity in the Bone Microenvironment as Characterized by Atomic Force Microscopy. *Biophys. J.* **119**, 502–513 (2020).
22. Calvi, L. M. *et al.* Osteoblastic cells regulate the haematopoietic stem cell niche. *Nature* **425**, 841–846 (2003).
23. Shen, B. *et al.* A mechanosensitive peri-arteriolar niche for osteogenesis and lymphopoiesis. *Nature* **2020**, (2021).
24. Salmerón-Sánchez, M. & Dalby, M. J. Synergistic growth factor microenvironments. *Chem. Commun.* **52**, 13327–13336 (2016).
25. Spencer, J. A. *et al.* Direct measurement of local oxygen concentration in the bone marrow of live animals. *Nature* **508**, 269–273 (2014).
26. Estrada, J. C. *et al.* Culture of human mesenchymal stem cells at low oxygen tension improves growth and genetic stability by activating glycolysis. *Cell Death Differ.* **19**, 743–55 (2012).
27. Guarnerio, J. *et al.* Bone Marrow Endosteal Mesenchymal Progenitors Depend on HIF Factors for Maintenance and Regulation of Hematopo. *Stem Cell Reports* **2**, 794–809 (2014).
28. Nakahara, F. *et al.* Engineering a haematopoietic stem cell niche by revitalizing mesenchymal stromal cells. *Nat. Cell Biol.* **21**, 560–567 (2019).
29. Leisten, I. *et al.* 3D co-culture of hematopoietic stem and progenitor cells and mesenchymal stem cells in collagen scaffolds as a model of the hematopoietic niche. *Biomaterials* **33**, 1736–1747 (2012).
30. Gilchrist, A. E. & Harley, B. A. C. Connecting secretome to hematopoietic stem cell phenotype shifts in an engineered bone marrow niche. *Integr. Biol.* **12**, 175–187 (2020).
31. Bourgine, P. E. *et al.* In vitro biomimetic engineering of a human hematopoietic niche with functional properties. *Proc. Natl. Acad. Sci.* **115**, E5688–E5695 (2018).

32. Rödling, L. *et al.* 3D models of the hematopoietic stem cell niche under steady-state and active conditions. *Sci. Rep.* 1–15 (2017) doi:10.1038/s41598-017-04808-0.
33. Chou, D. B. *et al.* On-chip recapitulation of clinical bone marrow toxicities and patient-specific pathophysiology. *Nat. Biomed. Eng.* **4**, (2020).
34. Doulatov, S., Notta, F., Laurenti, E. & Dick, J. E. Hematopoiesis: A human perspective. *Cell Stem Cell* **10**, 120–136 (2012).
35. Llopis-hernández, V. *et al.* Material-driven fibronectin assembly for high-efficiency presentation of growth factors. *Sci. Adv.* 1–11 (2016) doi:10.1126/sciadv.1600188.
36. Cheng, Z. A. *et al.* Nanoscale Coatings for Ultralow Dose BMP-2-Driven Regeneration of Critical-Sized Bone Defects. *Adv. Sci.* **1800361**, 1800361 (2018).
37. Itkin, T. *et al.* Distinct bone marrow blood vessels differentially regulate haematopoiesis. *Nature* 1–19 (2016) doi:10.1038/nature17624.
38. Asada, N. *et al.* Differential cytokine contributions of perivascular haematopoietic stem cell niches. (2017) doi:10.1038/ncb3475.
39. Nilsson, S. K. *et al.* Immunofluorescence characterization of key extracellular matrix proteins in murine bone marrow in situ. *J. Histochem. Cytochem.* **46**, 371–377 (1998).
40. Choi, J. S. & Harley, B. A. C. Marrow-inspired matrix cues rapidly affect early fate decisions of hematopoietic stem and progenitor cells. *Sci. Adv.* **3**, (2017).
41. Früh, S. M., Schoen, I., Ries, J. & Vogel, V. Molecular architecture of native fibronectin fibrils. *Nat. Commun.* **6**, 7275 (2015).
42. Klotzsch, E. *et al.* Fibronectin forms the most extensible biological fibers displaying switchable force-exposed cryptic binding sites. *Proc. Natl. Acad. Sci. U. S. A.* **106**, 18267–18272 (2009).
43. Bieniek, M., Llopis-Hernandez, V., Douglas, K., Salmeron-Sanchez, M. & Lorenz, C. Minor chemistry changes alter surface hydration to control fibronectin adsorption and assembly into nanofibrils. *Adv. Theory Simulations* **1900169**, 1–13 (2019).
44. Martino, M. M. & Hubbell, J. A. The 12th-14th type III repeats of fibronectin function as a highly promiscuous growth factor-binding domain. *FASEB J.* **24**, 4711–4721 (2010).
45. Park, D. *et al.* Nestin is required for the proper self-renewal of neural stem cells. *Stem Cells* **28**, 2162–2171 (2010).
46. Le Blanc, K. & Mougiakakos, D. Multipotent mesenchymal stromal cells and the innate immune system. *Nat. Rev. Immunol.* **12**, 383–396 (2012).
47. Dorronsoro, A. *et al.* Intracellular role of IL-6 in mesenchymal stromal cell immunosuppression and proliferation. *Sci. Rep.* **10**, 1–12 (2020).
48. Haghighitalab, A. *et al.* Investigating the effects of IDO1, PTGS2, and TGF-β1 overexpression on immunomodulatory properties of hTERT-MSCs and their extracellular vesicles. *Sci. Rep.* **11**, 1–19 (2021).
49. He, Y. *et al.* Mesenchymal stem cell deficiency influences megakaryocytopoiesis through the TNFAIP3/NF-κB/SMAD pathway in patients with immune thrombocytopenia. *Br. J. Haematol.* **180**, 395–411 (2018).
50. Shen, S. P. *et al.* EphA2 is a biomarker of hMSCs derived from human placenta and umbilical cord. *Taiwan. J. Obstet. Gynecol.* **54**, 749–756 (2015).
51. Weidemann, A. & Johnson, R. S. Biology of HIF-1 a. 621–627 (2008) doi:10.1038/cdd.2008.12.
52. Pattappa, G., Heywood, H. K., de Bruijn, J. D. & Lee, D. A. The metabolism of human mesenchymal stem cells during proliferation and differentiation. *J. Cell. Physiol.* **226**,

2562–2570 (2011).
53. Vander Heiden, M. G., Cantley, L. C. & Thompson, C. . Understanding the Warburg Effect: the metabolic requirements of cell proliferation. *Science (80-.).* **324**, 1029–1033 (2009).
54. Sahlgren, C. M. *et al.* Cdk5 regulates the organization of Nestin and its association with p35. *Mol. Cell. Biol.* **23**, 5090–5106 (2003).
55. Pallari, H.-M. *et al.* Nestin as a regulator of Cdk5 in differentiating myoblasts. *Mol. Biol. Cell* **22**, 1539–1549 (2011).
56. Sahlgren, C. M. *et al.* A nestin scaffold links Cdk5/p35 signaling to oxidant-induced cell death. *EMBO J.* **25**, 4808–4819 (2006).
57. Galleu, A. *et al.* Apoptosis in mesenchymal stromal cells induces in vivo recipient-mediated immunomodulation. *Sci. Transl. Med.* **9**, 1–12 (2017).
58. Shentu, Y. *et al.* Nestin Promotes Peritoneal Fibrosis by Protecting HIF1-α From Proteasomal Degradation. *Front. Physiol.* **11**, 1–11 (2020).
59. Wu, Y. *et al.* Highly efficient therapeutic gene editing of human hematopoietic stem cells. *Nat. Med.* **25**, 776–783 (2019).
60. Grassinger, J., Haylock, D. N., Williams, B., Olsen, G. H. & Nilsson, S. K. Phenotypically identical hemopoietic stem cells isolated from different regions of bone marrow have different biologic potential. *Blood* **116**, 3185–3196 (2010).
61. Ross, E. A. *et al.* Nanotopography reveals metabolites that maintain the immunosuppressive phenotype of mesenchymal stem cells. *BioRxiv* (2019).
62. Wilson, A. *et al.* Hematopoietic Stem Cells Reversibly Switch from Dormancy to Self-Renewal during Homeostasis and Repair. *Cell* **135**, 1118–1129 (2008).
63. Chaudhuri, O. *et al.* Hydrogels with tunable stress relaxation regulate stem cell fate and activity. *Nat. Mater.* (2015) doi:10.1038/nmat4489.
64. Martin, M. Cutadapt removes adapter sequences from high-throughput sequencing reads. *EMBnet.journal* **17**, 10 (2011).
65. Bray, N. L., Pimentel, H., Melsted, P. & Pachter, L. Near-optimal probabilistic RNA-seq quantification. *Nat. Biotechnol.* **34**, 525–527 (2016).
66. Love, M. I., Huber, W. & Anders, S. Moderated estimation of fold change and dispersion for RNA-seq data with DESeq2. *Genome Biol.* **15**, 1–21 (2014).
67. Westrop, G. D. *et al. Metabolomic profiling and stable isotope labelling of Trichomonas vaginalis and Tritrichomonas foetus reveal major differences in amino acid metabolism including the production of 2-hydroxyisocaproic acid, cystathionine and S-methylcysteine*. *PLoS ONE* vol. 12 (2017).
68. Chokkathukalam, A. *et al.* MzMatch-ISO: An R tool for the annotation and relative quantification of isotope-labelled mass spectrometry data. *Bioinformatics* **29**, 281–283 (2013).
69. Brinkman, E. K., Chen, T., Amendola, M. & Van Steensel, B. Easy quantitative assessment of genome editing by sequence trace decomposition. *Nucleic Acids Res.* **42**, 1–8 (2014).

Supplementary Information

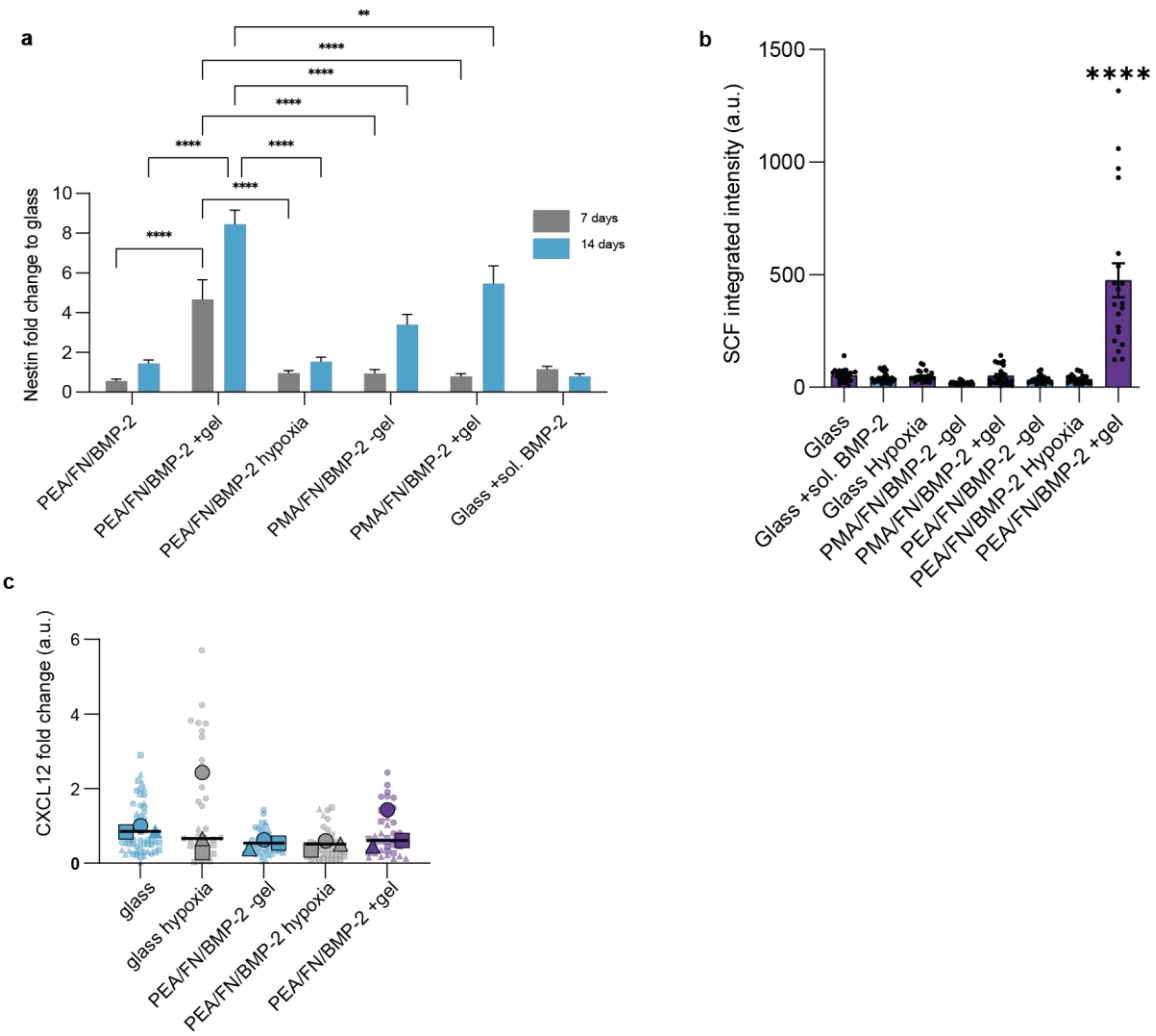

Supplementary Figure 1| ***Perivascular stromal cell niche phenotype. a****, Nestin expression measured by immunofluorescence at day 7 and 14 of culture. Nestin expression significantly increased in perivascular stromal cells on the PEA system only in the presence of low stiffness gels (+gel niche). PMA is used as a control polymer and shows some increase with gel only by day 14. Glass with soluble BMP-2 (50 ng/ml) added to the media is used as a further control and shows the addition of soluble, not matrix bound, BMP-2 does not induce nestin expression. Graph shows mean integrated intensity as fold change to glass control ± SEM, ****= p<0.001, **= p<0.005,determined by one-way ANOVA followed by Tukey's multiple comparison test. n = 4 material replicates.* ***b,*** *SCF and c, CXCL12 production in niche models. Cells were cultured in niche systems for 14 days with brefeldin A treatment (5 μg/ml in culture media) added for the final 24h to inhibit intracellular protein transport. Quantification of immunofluorescence staining with b, anti-SCF shows significant increase only in the PEA/FN/BMP-2 +gel condition. Graph shows mean ± SEM, ****= p<0.001, determined by one-way ANOVA followed by Tukey's multiple comparison test. Each point represents integrated SCF intensity of 1ximage field/number nuclei, from 4 material replicates. For* ***c****, CXCL12 revealed all conditions expressed CXCL12, but with no significant differences. Graph shows mean integrated intensity CXCL12 as fold change to glass control (n=3 material replicates, for 3 independent experiments with different donor cells), each point represents 1x image field/number nuclei. Non-significant, determined by one-way ANOVA followed by Tukey's multiple comparison test.*

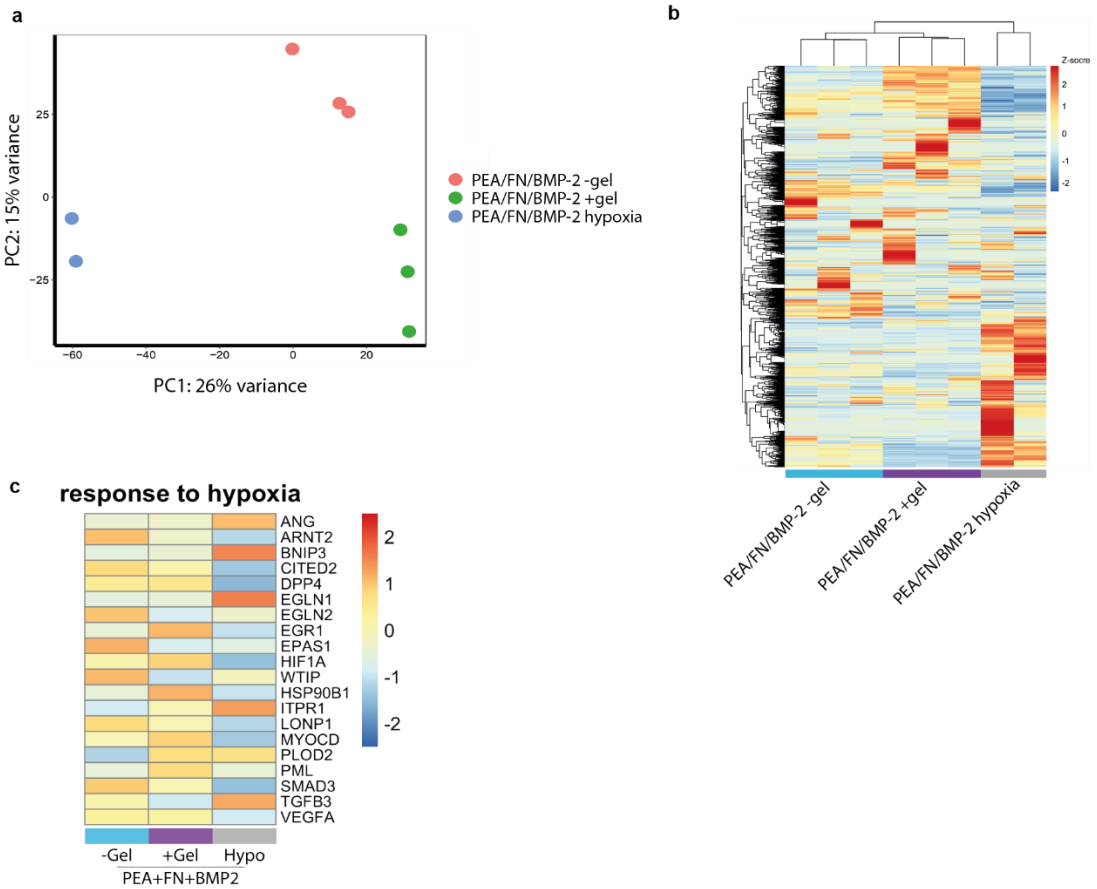

Supplementary Figure 2| ***RNA-seq analysis of PerSC niche phenotype at day 7. a,*** *Principal component analysis (PCA) shows transcripts from conditions PEA/FN/BMP-2 -gel/+gel/hypoxia samples cluster independently.* ***b,*** *Heatmap of z-scored changes in transcript levels.* ***c,*** *z-scored changes in transcript levels of genes involved in GO enrichment pathway 'response to hypoxia'. Genes with FDR < = 0.05 were considered as differentially enriched. N = 3 material replicates, for hypoxia n=2 material replicates as one replicate failed RNA quality control.*

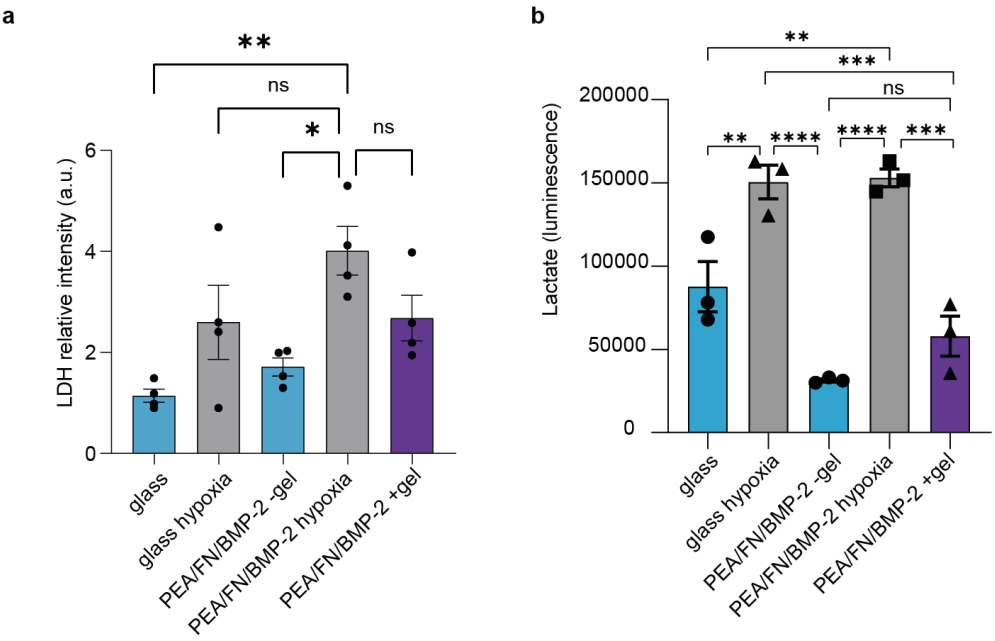

Supplementary Figure 3| ***Lactate dehydrogenase and lactate levels are not raised with PEA/FN/BMP-2 +gel. a****, in-cell western analysis of lactate dehydrogenase (LDH) levels in cells detected by immunofluorescence at day 7. Cell in PEA/FN/BMP-2 with hypoxia had significantly increased levels of the enzyme. Graph shows fluorescent intensity of LDH normalised to cell number (CellTag800) ± SEM, *= p<0.05, **= p<0.005, determined by one-way ANOVA followed by Tukey's multiple comparison test. N = 4 material replicates.* ***b****, Lactate levels in cell supernatant at day 14 measured by luminescence. Glass and PEA/FN/BMP-2 hypoxia samples had significantly raised levels. Graph shows n= 4 material replicates, ± SEM, **= p<0.005, ***= p<0.001, ****= p<0.001 determined by one-way ANOVA followed by Tukey's multiple comparison test.*

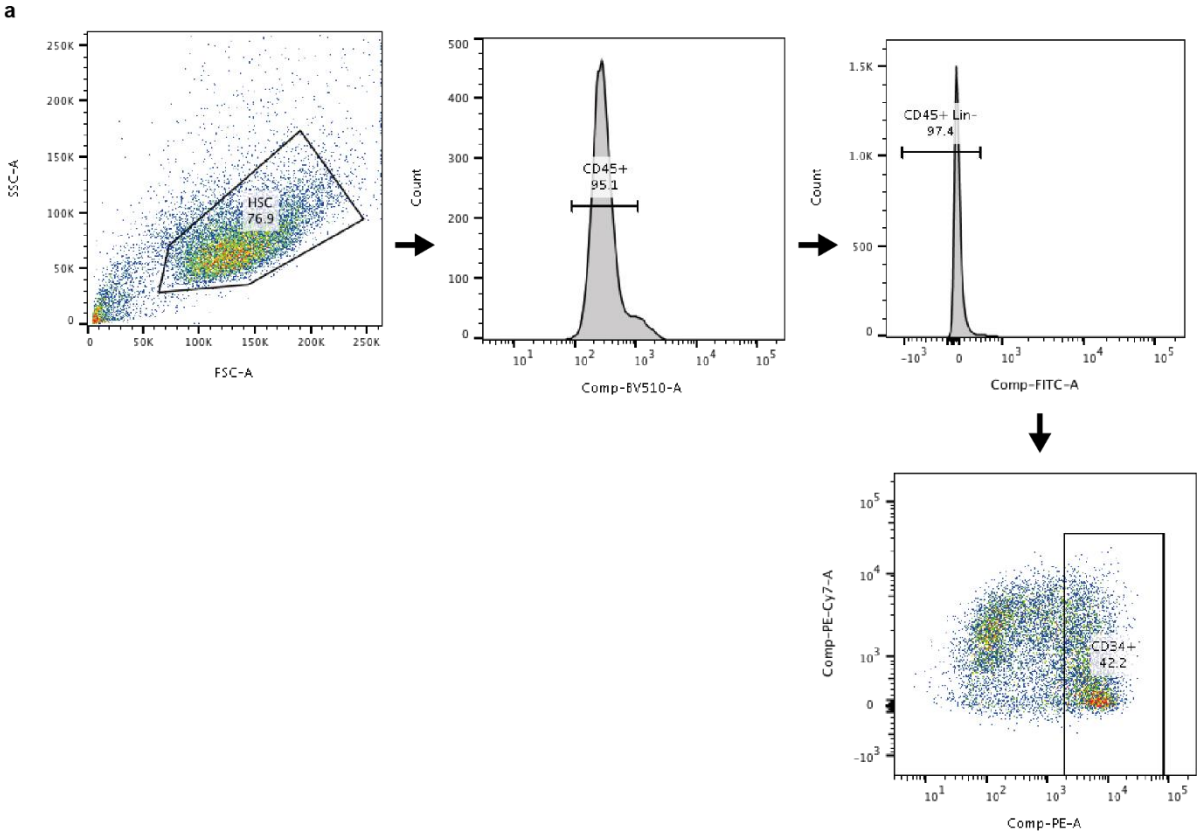

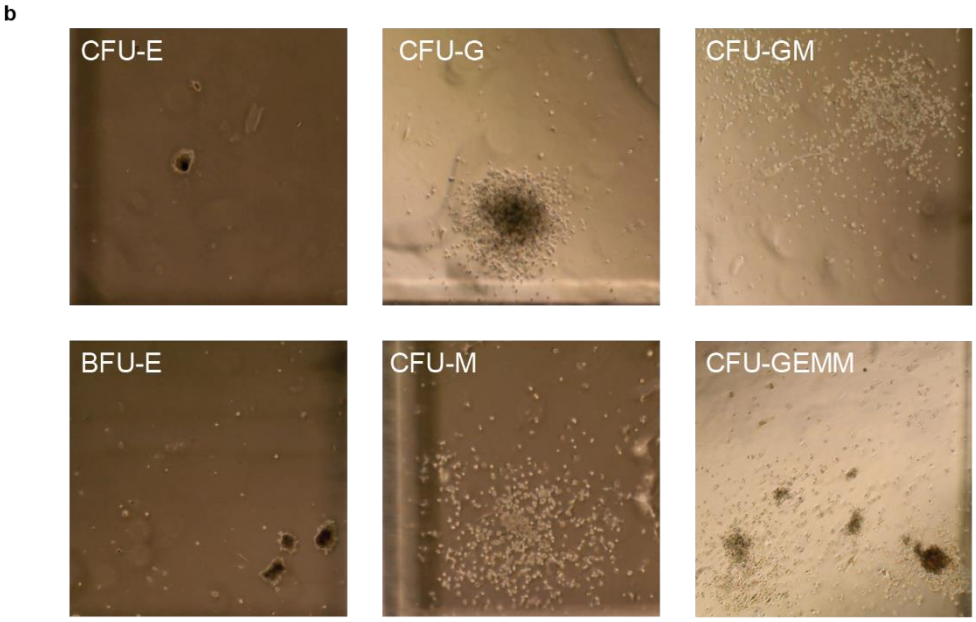

Supplementary Figure 4| ***LTC-IC FACS gating strategy and colony phenotyping. a****, Sample data taken from -gel conditions, patient 1. FSC-A versus SSC-A plot used to identify viable cells; gate added on CD45^{+ve} cells to remove any PerSCs; Lin^{-ve} gate used to remove any committed progenitors and final gate added on CD34^{+ve} population. These cells were collected and used in the LTC-IC assay.* ***b****, Representative colony types in colony forming unit (CFU) assay after 7 days. CFU-E; contain ~8-200 haemoglobinised erythroblasts. BFU-E; clusters of erythroid progenitors with high proliferative capacity. CFU-G; homogenous population of granulocyte progenitors. CFU-M; homogenous population of macrophage progenitors. CFU-GM; heterogenous population of macrophages and granulocytes. CFU-GEMM; multilineage progenitors that give rise to erythroid, granulocyte, macrophage and megakaryocyte lineages.*

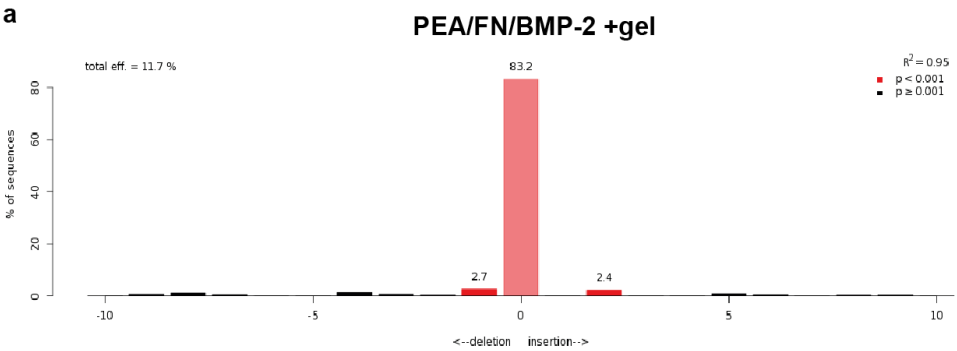

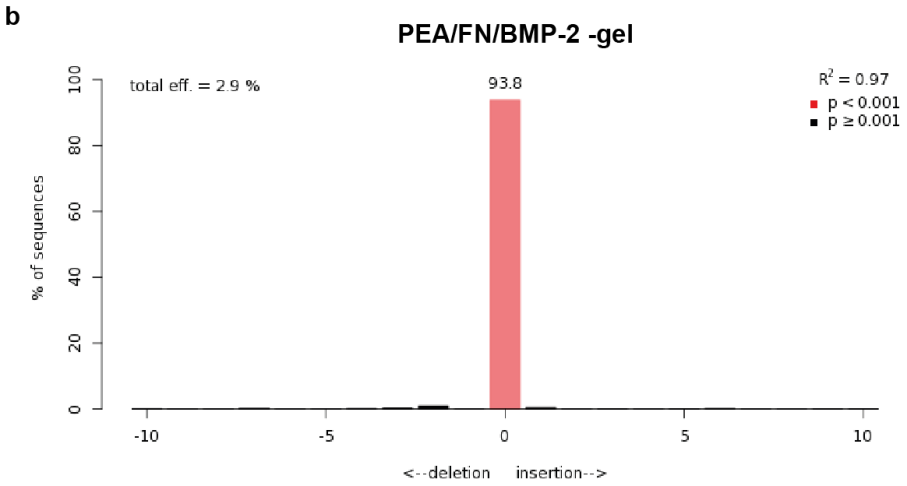

*Supplementary Figure 5|****TIDE analysis of CRISPR-edited HSCs after co-culture in niches.*** *CD34+ cells were edited using CRISPR targeting the AAVS1 locus and co-cultured in control gold standard media, or in niche models, for 5 days post-editing. Culture in PEA+gel niches enhanced editing,* ***a*** *&* ***c****, shows indel spectrum for PEA+gel and PEA-gel HSCs cultured in 0% media, respectively.* ***b*** *&* ***d****, show aberrant sequence signal of PEA+gel and PEA-gel 0% media, respectively.*

Supplementary table 1| Differentiation-related genes of interest.

TGF, transforming growth factor; MSC, mesenchymal stem cell; BMP, bone morphogenetic protein, SMAD, mothers against decapentaplegic; ERK, extracellular related kinase.

Gene	Definition	Summary	Supp refs
BDNF	Brain-Derived Neurotrophic Factor	Neurogenesis modulator.	1,2

BMP2	Bone Morphogenetic Protein-2	TGF-β superfamily member signalling molecules, involved in bone formation.	[3–5]
RUNX2	Runt-Related Transcription Factor-2	Transcriptional master regulator of osteogenesis in MSCs.	[6–8]
SMAD4	SMAD Family Member 4	Involved in canonical BMP signalling.	[9]
BMP6	Bone Morphogenetic Protein-6	TGF-β superfamily member signalling molecules, expressed in hypertrophic cartilage.	[5,10]
GFAP	Glial Fibrillary Acidic Protein	Intermediate filament protein found in astroglia cytoskeleton.	[11,12]
BGLAP	Osteocalcin	Expressed and secreted by osteoblasts.	[8,13–15]
BMP4	Bone Morphogenetic Protein 4	TGF-β superfamily member, role in embryogenesis and osteogenesis.	[5,16,17]
ALPP	Alkaline Phosphatase	Metalloenzyme, catalyses hydrolysis of phosphoric acid monoesters. Involved in bone formation.	[7,8]
SP7	Osterix	Bone-specific transcription factor. Required for osteoblast differentiation.	[18]
ADIPOQ	Adiponectin	Adipocyte-specific secretory protein.	[19–21]
TGFB3	Transforming Growth Factor Beta 3	Bind TGF-β receptors and activate SMAD signalling.	[9,22]
EGF	Epidermal Growth Factor	Role in growth, proliferation and differentiation of several cell types.	[23]
VWF	Von Willebrand Factor	Haemostatic plasma glycoprotein, expressed by endothelial cells and some HSCs.	[22,24,25]
SPARC	Osteonectin	Matrix-associated protein required for collagen calcification in bone.	[26]
BMPR1A	Bone Morphogenetic Protein Receptor Type 1A	Transmembrane serine/threonine kinase receptors for TGF-β superfamily ligands. Involved in bone formation.	[7,27]
ALPL	Alkaline Phosphatase, Biomineralization Associated	Metalloenzyme, catalyses hydrolysis of phosphoric acid monoesters. Involved in bone formation.	[7,8]
PPARG	Peroxisome Proliferator Activated Receptor Gamma	Master regulator of adipocyte differentiation.	[28]
BMPR2	Bone Morphogenetic Protein Receptor Type 2	Transmembrane serine/threonine kinase receptors for TGF-β superfamily ligands. Involved in SMAD signalling.	[29,30]
COL1A1	Collagen Type I Alpha Chain	Pro-alpha chains of type I collagen.	[7]
SOX9	SRY-Box Transcription Factor 9	Master regulator of chondrogenic differentiation in MSCs.	[31]
BMP7	Bone Morphogenetic Protein 7	TGF-β superfamily member signalling molecule, promotes osteoblast differentiation.	[32,33]
FGF10	Fibroblast Growth Factor 10	Role in cell division, proliferation, differentiation and survival. Important in development.	[34]
BMPR1B	Bone Morphogenetic Protein Receptor Type 1B	Transmembrane serine/threonine kinase receptors for TGF-β superfamily ligands. Involved in SMAD signalling.	[35]
SPP1	Osteopontin	Non-collagenous protein present in bone matrix.	[8,36,37]

FGF2	Fibroblast Growth Factor 2	Role in cell division, proliferation, differentiation and survival. Can signal through ERK to activate RUNX2.	[38]

Supplementary table 2| Niche-related genes of interest.
BM, bone marrow; HSC, hematopoietic stem cell; MSC, mesenchymal stem cell; ECM, extracellular matrix; VEGF, vascular endothelial growth factor; ESC, embryonic stem cell.

Gene	Definition	Summary	Supp refs
CDH2	Cadherin 2	Expressed by osteolineage cells in the BM niche.	[39–43]
ALCAM	Activated Leukocyte Cell Adhesion Molecule	MSC/PerSC marker.	[24,44]
ITGAV	Integrin Subunit Alpha V	Expressed by nestin+ perivascular stromal cells in the BM niche.	[44]
CSPG4	Chondroitin Sulphate Proteoglycan 4 (NG2; Nerve/Glial antigen 2)	Expressed by arteriole lining PerSCs in the BM niche.	[45–47]
JAG1	Jagged Canonical Notch Ligand 1	Expressed by BM stromal cells and osteoblasts. May activate Notch signalling in HSCs.	[47,48]
KITLG	KIT Ligand	Stem Cell Factor (SCF); HSC maintenance growth factor produced by Lepr+ and Nestin+ stromal and endothelial cells in the niche.	[49]
LIF	Leukaemia Inhibitory Factor	Interleukin-6 family cytokine, important in haematopoietic differentiation and regulation.	[50,51]
ITGB1	Integrin Subunit Beta 1	Expressed by HSCs and MSCs in the BM niche.	[4,52,53]
PDGFRA	Platelet Derived Growth Factor Receptor Alpha	Expressed by a subset of CD51+ stromal cells in the BM niche that correspond to increased nestin expression.	[44]
MMP2	Matrix Metallopeptidase 2	Shown to release CXCL12 from the ECM.	[54–56]
ICAM1	Intercellular Adhesion Molecule 1	Expressed by immunomodulatory MSCs and by sinusoidal endothelial cells in the BM niche.	[22,57]
CXCL12	C-X-C Motif Chemokine Ligand 12	Stromal Cell-Derived Factor 1(SDF-1). HSC regulatory cytokine produced by nestin+ perivascular cells in the BM niche.	[46]
ITGAX	Integrin Subunit Alpha X	Expressed in the BM niche by lymphocytes.	[58]
PDGFRB	Platelet Derived Growth Factor Receptor Beta	Expressed by endothelial cells lining BM arterioles and sinusoids.	[49]
LEPR	Leptin Receptor	Expressed by sinusoid-associated cells in the bone marrow niche.	[45–47]
VCAM1	Vascular Cell Adhesion Molecule 1	Involved in blood cell retention in the BM niche, ligands is integrinβ1.	[46,49]
NOTCH1	Notch Receptor 1	Roles in osteoblast and hematopoietic cell differentiation and maturation.	[59–61]
MCAM	Melanoma Cell Adhesion Molecule (CD146)	Marker for PerSCs and stromal stem cells.	[24,44]

NCAM1	Neural Cell Adhesion Molecule 1	Considered an early neural progenitor marker – correlated with nestin expression.	[62]
NES	Nestin	Nestin+ PerSCs and stromal cells regulate HSC activity in the BM niche.	[44,45,47,63–65]
THY1	Thy-1 Cell Surface Antigen	CD90; Involved in early BM niche development, used as MSC/HSC marker.	[66–68]
CSF2	Colony Stimulating Factor 2	Granulocyte macrophage-colony stimulating factor (GM-CSF). Produced in multiple cell types the BM niche.	[69,70]
KDR	Kinase Insert Domain Receptor	VEGF receptor. MSC marker.	[71,72]
THPO	Thrombopoietin	Osteoblast-derived HSC maintenance cytokine.	[73]
NGFR	Nerve Growth Factor Receptor	MSC marker.	[74]
VIM	Vimentin	Intermediate filament protein expressed in mesenchymal cells. Polymerisation partner of nestin.	[75]
POU5F1	Octamer-Binding Protein 4	Regulates self-renewal and differentiation in MSCs. Shown to be regulated by hypoxia in cultured ESCs.	[76,77]
VEGFA	Vascular Endothelial Growth Factor A	Regulator of blood vessel formation. Required for HSC survival. Produced in hypoxia.	[78]

Supplementary table 3**| Flow cytometry antibodies for PerSC phenotyping.**

Marker	Fluorophore	Clone	Supplier
Lepr	APC (panel 1)	REA361	Miltenyi Biotech
CD51	APC (panel 2)	NKI-M9	Biolegend
CD90	APC-Cy7 (panel 1)	5E10	Thermo Fisher, eBioscience
CD31	APC-Cy7 (panel 2)	WM59	Thermo Fisher, eBioscience
CD29	FITC (panel 1)	TS2/16	Thermo Fisher, eBioscience
NG2	PE (panel 1)	7.1	Thermo Fisher, eBioscience
CD140a	PE (panel 2)	16A1	Thermo Fisher, eBioscience
CD146	PerCP-Cy5.5 (panel 1)	P1H12	Biolegend
CD166	PerCP-eFluor710 (panel 2)	3A6	Thermo Fisher, eBioscience
CD140b	PE-Cy7 (panel 2)	APB5	Thermo Fisher, eBioscience
CD105	eFluor 450 (panel 2)	SN6	Thermo Fisher, eBioscience

Supplementary table 4**| Flow cytometry antibodies for HSC phenotyping and LTC-IC assay sorting.**

Marker	Fluorophore	Clone	Supplier
CD34	PE	4H11	Thermo Fisher, eBioscince
CD45	APC-Cy7	2D1	BD Biosciences
CD38	PE-Cy7	HB7	Thermo Fisher, eBioscince
Lineage cocktail	FITC	-	Thermo Fisher, eBioscince

Supplementary references

1. Reyes, J. H. *et al.* Glutamatergic neuronal differentiation of mouse embryonic stem cells after transient expression of neurogenin 1 and treatment with BDNF and GDNF: In vitro and in vivo studies. *J. Neurosci.* **28**, 12622–12631 (2008).
2. Fuentealba, L. C., Obernier, K. & Alvarez-Buylla, A. Adult neural stem cells bridge their niche. *Cell Stem Cell* **10**, 698–708 (2012).
3. Dobre, O. *et al.* A Hydrogel Platform that Incorporates Laminin Isoforms for Efficient Presentation of Growth Factors – Neural Growth and Osteogenesis. *Adv. Funct. Mater.* **31**, (2021).
4. Martino, M. M. *et al.* Engineering the growth factor microenvironment with fibronectin domains to promote wound and bone tissue healing. *Sci. Transl. Med.* **3**, 100ra89 (2011).
5. Chen, D., Zhao, M. & Mundy, G. R. Bone morphogenetic proteins. *Growth Factors* **22**, 233–241 (2004).
6. Bruderer, M., Richards, R. G., Alini, M. & Stoddart, M. J. Role and regulation of runx2 in osteogenesis. *Eur. Cells Mater.* **28**, 269–286 (2014).
7. Long, F. Building strong bones: Molecular regulation of the osteoblast lineage. *Nat. Rev. Mol. Cell Biol.* **13**, 27–38 (2012).
8. Yang, J. *et al.* Nanotopographical Induction of Osteogenesis through Adhesion, Bone Morphogenic Protein Cosignaling, and Regulation of MicroRNAs. *ACS Nano* **8**, 9941–9953 (2014).
9. Heldin, C.-H., Kohei, M. & Peter, D. TFG-beta signalling from cell membrane to nucleas through SMAD proteins. *Nature* **390**, 465–71 (1997).
10. Kugimiya, F. *et al.* Involvement of endogenous bone morphogenetic protein (BMP) 2 and BMP6 in bone formation. *J. Biol. Chem.* **280**, 35704–35712 (2005).
11. Hol, E. M. & Pekny, M. Glial fibrillary acidic protein (GFAP) and the astrocyte intermediate filament system in diseases of the central nervous system. *Curr. Opin. Cell Biol.* **32**, 121–130 (2015).
12. Yamazaki, S. *et al.* Nonmyelinating schwann cells maintain hematopoietic stem cell hibernation in the bone marrow niche. *Cell* **147**, 1146–1158 (2011).
13. Moser, S. C. & van der Eerden, B. C. J. Osteocalcin — A versatile bone-derived hormone. *Front. Endocrinol. (Lausanne).* **10**, 4–9 (2019).
14. Dalby, M. J., Gadegaard, N. & Oreffo, R. O. C. Harnessing nanotopography and integrin-matrix interactions to influence stem cell fate. *Nat. Mater.* **13**, 558–569 (2014).
15. Curran, J. M., Chen, R. & Hunt, J. A. The guidance of human mesenchymal stem cell differentiation in vitro by controlled modifications to the cell substrate. *Biomaterials* **27**, 4783–4793 (2006).
16. Goldman, D. C. *et al.* BMP4 regulates the hematopoietic stem cell niche. *Blood* **114**, 4393–4401 (2009).
17. Re'Em, T., Witte, F., Willbold, E., Ruvinov, E. & Cohen, S. Simultaneous regeneration of articular cartilage and subchondral bone induced by spatially presented TGF-beta and BMP-4 in a bilayer affinity binding system. *Acta Biomater.* **8**, 3283–3293 (2012).
18. Nakashima, K. *et al.* The Novel Zinc Finger-Containing Transcription Factor Osterix Is Required for Osteoblast Differentiation and Bone Formation. *Cell* **108**, 17–29 (2002).
19. Yokota, T. *et al.* Adiponectin, a new member of the family of soluble defense collagens, negatively regulates the growth of myelomonocytic progenitors and the functions of macrophages. *Blood* **96**, 1723–32 (2000).
20. Maeda, K. *et al.* cDNA Cloning and Expression of a Novel Adipose Specific Collagen-like Factor, apM1 (dioseost Abundant Gene Transcript 1). *Biochem. Biophys. Res. Commun.* **221**, 286–289 (1996).
21. Saraiva, L. R. *et al.* Adipocyte Accumulation in the Bone Marrow during Obesity and Aging Impairs Stem Cell-Based Hematopoietic and Bone Regeneration. *Cell Stem Cell* **20**, 771-784.e6 (2017).

22. Xu, C. *et al.* Stem cell factor is selectively secreted by arterial endothelial cells in bone marrow. *Nat. Commun.* **9**, 1–13 (2018).
23. Krampera, M. *et al.* HB-EGF/HER-1 signaling in bone marrow mesenchymal stem cells: Inducing cell expansion and reversibly preventing multilineage differentiation. *Blood* **106**, 59–66 (2005).
24. Crisan, M. *et al.* A Perivascular Origin for Mesenchymal Stem Cells in Multiple Human Organs. *Cell Stem Cell* **3**, 301–313 (2008).
25. Pinho, S. *et al.* Lineage-Biased Hematopoietic Stem Cells Are Regulated by Distinct Niches. *Dev. Cell* **44**, 634-641.e4 (2018).
26. Termine, J. D. *et al.* Osteonectin, a bone-specific protein linking mineral to collagen. *Cell* **26**, 99–105 (1981).
27. Cheng, Z. A. *et al.* Nanoscale Coatings for Ultralow Dose BMP-2-Driven Regeneration of Critical-Sized Bone Defects. *Adv. Sci.* **1800361**, 1800361 (2018).
28. Lehrke, M. & Lazar, M. A. The many faces of PPARγ. *Cell* **123**, 993–999 (2005).
29. Lowery, J. W. *et al.* Loss of BMPR2 leads to high bone mass due to increased osteoblast activity. *J. Cell Sci.* **128**, 1308–1315 (2015).
30. Lavery, K., Swain, P., Falb, D. & Alaoui-Ismaili, M. H. BMP-2/4 and BMP-6/7 differentially utilize cell surface receptors to induce osteoblastic differentiation of human bone marrow-derived mesenchymal stem cells. *J. Biol. Chem.* **283**, 20948–20958 (2008).
31. Bi, W., Deng, J. M., Zhang, Z., Behringer, R. R. & De Crombrugghe, B. Sox9 is required for cartilage formation. *Nat. Genet.* **22**, 85–89 (1999).
32. Piccolo, S., Sasai, Y., Lu, B. & De Robertis, E. M. Dorsoventral patterning in Xenopus: Inhibition of ventral signals by direct binding of chordin to BMP-4. *Cell* **86**, 589–598 (1996).
33. Ducy, P., Zhang, R., Geoffroy, V., Ridall, A. L. & Karsenty, G. Osf2/Cbfa1: A transcriptional activator of osteoblast differentiation. *Cell* **89**, 747–754 (1997).
34. Watson, J. & Francavilla, C. Regulation of FGF10 Signaling in Development and Disease. *Front. Genet.* **9**, 1–10 (2018).
35. Shi, C. *et al.* Deletion of BMP receptor type IB decreased bone mass in association with compromised osteoblastic differentiation of bone marrow mesenchymal progenitors. *Sci. Rep.* **6**, 1–13 (2016).
36. Noda, M. & Denhardt, D. T. Chapter 18 - Osteopontin. *Princ. Bone Biol.* 351–366 (2008).
37. Mark, M. P. *et al.* Immunohistochemical Phosphoprotein Demonstration of a 44-lcD in Developing Rat Bones1 that picture. *J. Histochem. Cytochem* (1987).
38. Park, O., Kim, H., Woo, K., Baek, J. & Ryoo, H. FGF2-activated ERK Mitogen-activated Protein Kinase Enhances Runx2 Acetylation and Stabilization *. **285**, 3568–3574 (2010).
39. Zhang, J. *et al.* Identification of the haematopoietic stem cell niche and control of the niche size. *Nature* **425**, 836–841 (2003).
40. Haug, J. S. *et al.* Article N-Cadherin Expression Level Distinguishes Reserved versus Primed States of Hematopoietic Stem Cells. 367–379 (2008) doi:10.1016/j.stem.2008.01.017.
41. Hosokawa, K. *et al.* Cadherin-Based Adhesion Is a Potential Target for Niche Manipulation to Protect Hematopoietic Stem Cells in Adult Bone Marrow. *Stem Cell* **6**, 194–198 (2010).
42. Kiel, M. J., Acar, M., Radice, G. L. & Morrison, S. J. Hematopoietic Stem Cells Do Not Depend on N-Cadherin to Regulate Their Maintenance. *Cell Stem Cell* **4**, 170–179 (2009).
43. Greenbaum, A. M., Revollo, L. D., Woloszynek, J. R., Civitelli, R. & Link, D. C. N-cadherin in osteolineage cells is not required for maintenance of hematopoietic stem cells. *Blood* **120**, 295–302 (2012).
44. Pinho, S. *et al.* PDGFR A and CD51 mark human stem cells capable of hematopoietic progenitor cell expansion. *J. Exp. Med.* **210**, 1351–1367 (2013).
45. Kunisaki, Y. *et al.* Arteriolar niches maintain haematopoietic stem cell quiescence. *Nature* **502**, 637–643 (2013).
46. Asada, N. *et al.* Differential cytokine contributions of perivascular haematopoietic stem cell niches. (2017) doi:10.1038/ncb3475.

47. Baccin, C. *et al.* Combined single-cell and spatial transcriptomics reveal the molecular, cellular and spatial bone marrow niche organization. *Nat. Cell Biol.* **22**, 38–48 (2020).
48. Calvi, L. M. *et al.* Osteoblastic cells regulate the haematopoietic stem cell niche. *Nature* **425**, 841–846 (2003).
49. Ding, L., Saunders, T. L., Enikolopov, G. & Morrison, S. J. Endothelial and perivascular cells maintain haematopoietic stem cells. *Nature* **481**, 457–62 (2012).
50. Escary, J., Perreau, J., Dumenilt, D., Ezine, S. & Brulet, P. Leukaemia inhibitory factor is necessary for maintenance of haematopoietic stem cells and thymocyte stimulation. **363**, 361–364 (1993).
51. Ranga, A. *et al.* 3D niche microarrays for systems-level analyses of cell fate. *Nat. Commun.* **5**, 1–10 (2014).
52. Hadland, B. *et al.* Engineering a niche supporting hematopoietic stem cell development using integrated single-cell transcriptomics. *Nat. Commun.* **13**, 1–17 (2022).
53. Williams, D. A., Rios, M., Stephens, C. & Patel, V. P. Fibronectin and VLA-4 in haematopoietic stem cell-microenvironment interactions. *Nature* **352**, 438–441 (1991).
54. Nyman, J. S. *et al.* Differential Effects Between the Loss of MMP-2 and MMP-9 on Structural and Tissue-Level Properties of Bone. **26**, 1252–1260 (2011).
55. Clutter, S. D., Fortney, J. & Gibson, L. F. MMP-2 is required for bone marrow stromal cell support of pro – B-cell chemotaxis. **33**, 1192–1200 (2005).
56. Saw, S., Weiss, A., Khokha, R. & Waterhouse, P. D. Metalloproteases : On the Watch in the Hematopoietic Niche. *Trends Immunol.* **40**, 1053–1070 (2019).
57. Ghannam, S., Pène, J., Torcy-moquet, G., Jorgensen, C. & Yssel, H. Mesenchymal Stem Cells Inhibit Human Th17 Cell Differentiation and Function and Induce a T Regulatory Cell Phenotype. (2022) doi:10.4049/jimmunol.0902007.
58. Villani, A. C. *et al.* Single-cell RNA-seq reveals new types of human blood dendritic cells, monocytes, and progenitors. *Science (80-.).* **356**, (2017).
59. Maillard, I. *et al.* Article Canonical Notch Signaling Is Dispensable for the Maintenance of Adult Hematopoietic Stem Cells. **1**, (2006).
60. Butler, J. M. *et al.* Endothelial Cells Are Essential for the Self-Renewal and Repopulation of Notch-Dependent Hematopoietic Stem Cells. *Cell Stem Cell* **6**, 251–264 (2010).
61. Mancini, S. J. C. *et al.* Jagged1-dependent Notch signaling is dispensable for hematopoietic stem cell self-renewal and differentiation. *Blood* **105**, 2340–2342 (2005).
62. Engler, A. J., Sen, S., Sweeney, H. L. & Discher, D. E. Matrix elasticity directs stem cell lineage specification. *Cell* **126**, 677–89 (2006).
63. Ding, L. & Morrison, S. J. Haematopoietic stem cells and early lymphoid progenitors occupy distinct bone marrow niches. *Nature* **495**, 231–235 (2013).
64. Ding, L., Saunders, T. L., Enikolopov, G. & Morrison, S. J. Endothelial and perivascular cells maintain haematopoietic stem cells. *Nature* **481**, 457–62 (2012).
65. Méndez-Ferrer, S. *et al.* Mesenchymal and haematopoietic stem cells form a unique bone marrow niche. *Nature* **466**, 829–834 (2010).
66. Chan, C. K. F. *et al.* Endochondral ossification is required for haematopoietic stem-cell niche formation. *Nature* **457**, 490–494 (2009).
67. Notta, F. *et al.* Isolation of Single Human Hematopoietic. *Science (80-.).* **333**, 218–222 (2011).
68. Maleki, M., Ghanbarvand, F. & Behvarz, M. R. Comparison of Mesenchymal Stem Cell Markers in Multiple Human Adult Stem Cells. **7**, 118–126 (2014).
69. Taichman, R., Reilly, M. J. & Emerson, S. G. Human osteoblasts support human hematopoietic progenitor cells in vitro bone marrow cultures. *Blood* **87**, 518–524 (1996).
70. Trapnell, B. C. & Abe, S. Colony stimulating factors. 540–546 (2004).
71. Cortés, F., Debacker, C., Péault, B. & Labastie, M. C. Differential expression of KDR/VEGFR-2 and CD34 during mesoderm development of the early human embryo. *Mech. Dev.* **83**, 161–164 (1999).

72. Blaber, E. A. *et al.* Mechanical unloading of bone in microgravity reduces mesenchymal and hematopoietic stem cell-mediated tissue regeneration. *Stem Cell Res.* **13**, 181–201 (2014).
73. Yoshihara, H. *et al.* Thrombopoietin/MPL Signaling Regulates Hematopoietic Stem Cell Quiescence and Interaction with the Osteoblastic Niche. *Cell Stem Cell* **1**, 685–697 (2007).
74. Kumar, A. *et al.* Specification and Diversification of Pericytes and Smooth Muscle Cells from Mesenchymoangioblasts. *Cell Rep.* **19**, 1902–1916 (2017).
75. Johnson, C. P., Tang, H., Carag, C., Speicher, D. W. & Discher, D. E. Forced Unfolding of Proteins Within Cells. *Science (80-.).* **317**, 663–667 (2007).
76. Forristal, C. E., Wright, K. L., Hanley, N. A., Oreffo, R. O. C. & Houghton, F. D. Hypoxia inducible factors regulate pluripotency and proliferation in human embryonic stem cells cultured at reduced oxygen tensions. *Reproduction* **139**, 85–97 (2010).
77. Tsai, C. C., Su, P. F., Huang, Y. F., Yew, T. L. & Hung, S. C. Oct4 and Nanog Directly Regulate Dnmt1 to Maintain Self-Renewal and Undifferentiated State in Mesenchymal Stem Cells. *Mol. Cell* **47**, 169–182 (2012).
78. Gerber, H., Malik, A. K., Solar, G. P. & Sherman, D. VEGF regulates haematopoietic stem cell survival by an internal autocrine loop mechanism. *Nature* **417**, 6–10 (2002).